

## Phase gate of one qubit simultaneously controlling $n$ qubits in a cavity

Chui-Ping Yang,<sup>1,2</sup> Yu-xi Liu,<sup>1,3,4</sup> and Franco Nori<sup>1,2</sup>

<sup>1</sup>*Advanced Science Institute, The Institute of Physical and Chemical Research (RIKEN), Wako-Shi, Saitama 351-0198, Japan*

<sup>2</sup>*Physics Department, The University of Michigan, Ann Arbor, Michigan 48109-1040, USA*

<sup>3</sup>*Institute of Microelectronics, Tsinghua University, Beijing 100084, China*

<sup>4</sup>*Tsinghua National Laboratory for Information Science and Technology (TNList), Tsinghua University, Beijing 100084, China*

(Received 27 July 2009; revised manuscript received 30 March 2010; published 17 June 2010)

We propose how to realize a three-step controlled-phase gate of one qubit simultaneously controlling  $n$  qubits in a cavity or coupled to a resonator. The  $n$  two-qubit controlled-phase gates, forming this multiqubit phase gate, can be performed simultaneously. The operation time of this phase gate is independent of the number  $n$  of qubits. This phase gate controlling at once  $n$  qubits is insensitive to the initial state of the cavity mode and can be used to produce an analogous CNOT gate simultaneously acting on  $n$  qubits. We present two alternative approaches to implement this gate. One approach is based on tuning the qubit frequency while in the other method the resonator frequency is tuned. Using superconducting qubits coupled to a resonator as an example, we show how to implement the proposed gate with one superconducting qubit simultaneously controlling  $n$  qubits selected from  $N$  qubits coupled to a resonator ( $1 < n < N$ ). We also give a discussion on realizing the proposed gate with atoms, by using one cavity initially in an arbitrary state.

DOI: [10.1103/PhysRevA.81.062323](https://doi.org/10.1103/PhysRevA.81.062323)

PACS number(s): 03.67.Lx, 42.50.Dv, 85.25.Cp

### I. INTRODUCTION

Quantum information processing has attracted considerable interest during the past decade. The building blocks of quantum computing are single-qubit and two-qubit logic gates. So far, a large number of theoretical proposals for realizing two-qubit gates in many physical systems, such as trapped ions, atoms in cavity QED, nuclear magnetic resonance (NMR), and solid-state devices, have been proposed. Moreover, two-qubit controlled-not (CNOT), controlled-phase (CP),  $i$ SWAP gates, or other two-qubit operations have been experimentally demonstrated in ion traps [1], NMR [2], quantum dots [3], and superconducting qubits [4–8].

In recent years, analogs of cavity QED have been studied using superconducting Josephson devices. There, a superconducting resonator provides a quantized cavity field, superconducting qubits act as artificial atoms, and the strong coupling between the field and superconducting qubits has been demonstrated [9]. Theoretically, many approaches for performing two-qubit logic gates using superconducting qubits coupled to a superconducting resonator or cavity have been proposed (see, e.g., [10–15]). Moreover, experimental demonstrations of two-qubit gates or two-qubit operations using superconducting qubits coupled to cavities have recently been reported [7,8].

Attention is now shifting to the physical realization of multiqubit gates (see, e.g., [16]) instead of just two-qubit gates. It is known that any multiqubit gate can be decomposed into two-qubit gates and one-qubit gates. When using the conventional gate-decomposition protocols to construct a multiqubit gate [17,18], the procedure usually becomes complicated as the number of qubits increases. Therefore, building a multiqubit gate may become very difficult since each elementary gate requires turning on and off a given Hamiltonian for a certain period of time, and each additional basic gate adds experimental complications and the possibility of more errors. During the past few years, several methods for constructing multiqubit phase gates with  $n$ -control qubits

acting on one target qubit based on ion traps [19], cavity QED [20,21], or circuit QED [22] have been proposed. As is well known, a multiqubit gate with multiple control qubits controlling a single qubit plays a significant role in quantum information processing, such as quantum algorithms (e.g., [23,24]) and quantum error-correction protocols [25].

In this work, we focus on another type of multiqubit gates, that is, a multiqubit phase gate with *one* control qubit simultaneously controlling  $n$  target qubits. This multiqubit gate is useful in quantum information processing such as entanglement preparation [26], error correction [27], quantum algorithms (e.g., the discrete cosine transform [28]), and quantum cloning [29]. In the following, we will propose a way for realizing this multiqubit gate using  $(n + 1)$  qubits in a cavity or coupled to a resonator. To implement this gate, we construct an effective Hamiltonian which contains interaction terms between the control qubit and each subordinate or target qubit. We will denote this  $n$ -target-qubit control-phase gate as an NTCP gate [Fig. 1(a)]. We present two alternative approaches to implement this NTCP gate. One approach is based on tuning the qubit frequency, while in the other method one tunes the cavity (or resonator) frequency. We present these two alternative methods because in some experimental implementations it might be easier to tune the qubit frequency, while in others tuning the cavity frequency might be preferable. For solid-state qubits such as superconducting qubits and semiconductor quantum dots, the qubit transition frequency (or the qubit level spacings) can be readily adjusted by varying the external parameters [30–34] (e.g., the external magnetic flux for superconducting charge qubits, the flux bias or current bias in the case of superconducting phase qubits and flux qubits [30–33], and the external electric field for semiconductor quantum dots [34]). Also, the cavity mode frequency can be changed in various experiments (e.g., [35–39]).

As shown in the following our proposal has several advantages: (i) The  $n$  two-qubit CP gates involved in the NTCP gate can be performed simultaneously; (ii) the operation time required for the gate implementation is independent of the

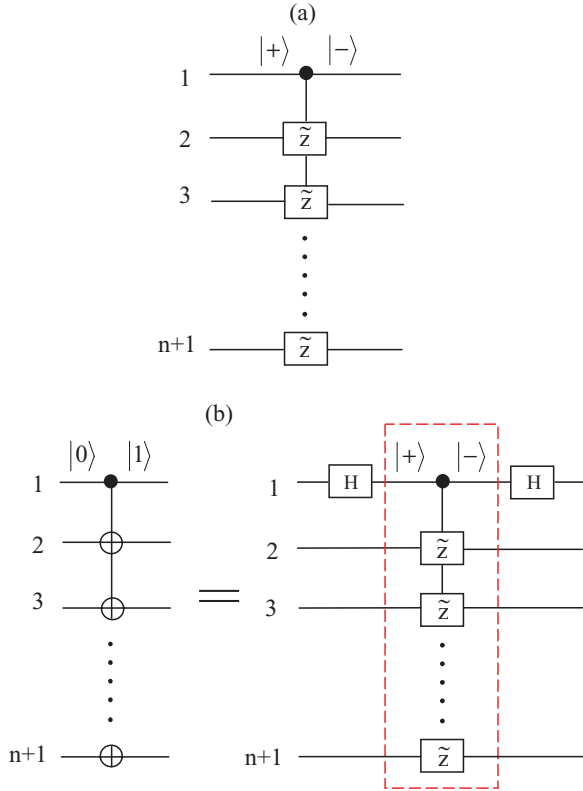


FIG. 1. (Color online) (a) Schematic circuit of an NTCP gate with qubit 1 simultaneously controlling  $n$  target qubits (2, 3,  $\dots$ ,  $n + 1$ ). The NTCP gate is equivalent to  $n$  two-qubit control phase (CP) gates, each having a shared control qubit (qubit 1) but a different target qubit (qubit 2, 3,  $\dots$ , or  $n + 1$ ). Here,  $\tilde{Z}$  represents a controlled-phase flip on each target qubit, with respect to the computational basis formed by the two eigenstates  $|+\rangle$  and  $|-\rangle$  of the Pauli operator  $\sigma_x$ . If the control qubit 1 is in the state  $|-\rangle$ , then the state  $|-\rangle$  at each  $\tilde{Z}$  is phase-flipped as  $|-\rangle \rightarrow -|-\rangle$  while the state  $|+\rangle$  remains unchanged. However, if the control qubit 1 is in the state  $|+\rangle$ , nothing happens to either of the states  $|+\rangle$  and  $|-\rangle$  at each  $\tilde{Z}$ . (b) The relationship between an  $n$ -target-qubit CNOT gate and an NTCP gate. The circuit on the left side of (b) is equivalent to the circuit on the right side of (b). For the circuit on the left side, the symbol  $\oplus$  represents a NOT gate on each target qubit, with respect to the computational basis formed by the two eigenstates  $|0\rangle$  and  $|1\rangle$  of the Pauli operator  $\sigma_z$ . If the control qubit 1 is in the state  $|1\rangle$ , then the state at  $\oplus$  is bit flipped as  $|1\rangle \rightarrow |0\rangle$  and  $|0\rangle \rightarrow |1\rangle$ . However, when the control qubit 1 is in the state  $|0\rangle$ , the state at  $\oplus$  remains unchanged. On the other hand, for the circuit on the right side, the part enclosed in the (red) dashed-line box represents an NTCP gate. The element containing H corresponds to a Hadamard transformation described by  $|0\rangle \rightarrow |+\rangle = (1/\sqrt{2})(|0\rangle + |1\rangle)$  and  $|1\rangle \rightarrow |-\rangle = (1/\sqrt{2})(|0\rangle - |1\rangle)$ .

number  $n$  of qubits; (iii) the proposal is insensitive to the initial state of the cavity mode, and thus no preparation for the initial state of the cavity mode is needed; (iv) no measurement on the qubits or the cavity mode is needed and thus the operation is simplified; and (v) the proposal requires only three steps of operations.

Note that a CNOT gate of one qubit simultaneously controlling  $n$  qubits, shown in Fig. 1(b), can also be achieved using the present proposal. This is because the  $n$ -target-qubit CNOT

gate is equivalent to an NTCP gate plus two Hadamard gates on the control qubit [Fig. 1(b)].

Our proposal demonstrates that a powerful phase gate of one qubit simultaneously controlling  $n$  qubits can be achieved in a cavity or resonator, which can be initially in an arbitrary state. This proposal is quite general and can be applied to physical systems such as trapped atoms, quantum dots, and superconducting qubits. We believe that this work is of general interest and significance because it provides a protocol for performing a controlled-phase (or controlled-not) gate with multiple target qubits.

This paper is organized as follows. In Sec. II, we introduce the  $n$ -target-qubit control phase gate studied in this work. In Sec. III, we discuss how to obtain the time-evolution operators for a qubit system interacting with a single cavity mode and driven by a classical pulse. In Sec. IV, using the time-evolution operators obtained, we present two alternative approaches for realizing the NTCP gate with qubits in a cavity or coupled to a resonator. In the Appendix, we provide guidelines on how to protect multilevel qubits from leaking out of the computational subspace. In Sec. V, using superconducting qubits coupled to a resonator, we show how to apply our general proposal to implement the proposed NTCP gate, and then discuss its feasibility based on current experiments in superconducting quantum circuits. In Sec. VI, we discuss how to extend the present proposal to implement the NTCP gate with trapped atomic qubits, by using one cavity. A concluding summary is provided in Sec. VII.

## II. ONE QUBIT SIMULTANEOUSLY CONTROLLING $N$ TARGET QUBITS

For two qubits, there are a total of four computational basis states, denoted by  $|++\rangle$ ,  $|+-\rangle$ ,  $|-+\rangle$ , and  $|--\rangle$ . Here,  $|+\rangle$  and  $|-\rangle$  are the two eigenstates of the Pauli operator  $\sigma_x$ . A two-qubit CP gate is defined as follows:

$$\begin{aligned} |++\rangle &\rightarrow |++\rangle, & |+-\rangle &\rightarrow |+-\rangle, & |-+\rangle &\rightarrow |-+\rangle, \\ |--\rangle &\rightarrow -|--\rangle, & & & & \end{aligned} \quad (1)$$

which implies that if and only if the control qubit (the first qubit) is in the state  $|-\rangle$ , a phase flip happens to the state  $|-\rangle$  of the target qubit (the second qubit), but nothing happens otherwise.

The NTCP gate considered here consists of  $n$  two-qubit CP gates [Fig. 1(a)]. Each two-qubit CP gate involved in this NTCP gate has a *shared* control qubit (labeled by 1) but a different target qubit (labeled by 2, 3,  $\dots$ , or  $n + 1$ ). According to the transformation (1) for a two-qubit CP gate, it can be seen that this NTCP gate with one control qubit (qubit 1) and  $n$  target qubits (qubits 2, 3,  $\dots$ ,  $n + 1$ ) can be described by the following unitary operator:

$$U = \prod_{j=2}^{n+1} (I_j - 2| -_1 -_j \rangle \langle -_1 -_j |), \quad (2)$$

where the subscript 1 represents the control qubit 1, while  $j$  represents the  $j$ th target qubit, and  $I_j$  is the identity operator for the qubit pair (1,  $j$ ), which is given by  $I_j = \sum_{rs} |r_1 s_j\rangle \langle r_1 s_j|$ , with  $r, s \in \{+, -\}$ . One can see that the operator (2) induces a phase flip (from the  $+$  sign to the  $-$  sign) to the logical state

$|-\rangle$  of each target qubit when the control qubit 1 is initially in the state  $|-\rangle$ , and nothing happens otherwise.

It should be mentioned that the NTCP gate can be defined by using the eigenstates  $|0\rangle$  and  $|1\rangle$  of the Pauli operator  $\sigma_z$ . However, we note that to construct a  $n$ -target CNOT gate (based on the NTCP gate defined in the eigenstates of  $\sigma_z$ ), a Hadamard gate acting on each target qubit before and after the NTCP gate (i.e., a total of  $2n$  Hadamard gates) would be required. In contrast, the construction of the  $n$ -target CNOT gate, using the NTCP gate defined in the eigenstates of  $\sigma_x$ , requires only two Hadamard gates [see Fig. 1(b)]. Therefore, the NTCP here, defined in the eigenstates of  $\sigma_x$ , makes the procedure for constructing an  $n$ -target CNOT gate much simpler.

### III. MODEL AND UNITARY EVOLUTION

Consider  $(n + 1)$  qubits interacting with the cavity mode and driven by a classical pulse. In the rotating-wave approximation, the Hamiltonian for the whole system is

$$H = H_0 + H_1 + H_2, \quad (3)$$

with

$$H_0 = -\frac{\hbar\omega_0}{2}S_z + \hbar\omega_c a^\dagger a, \quad (4)$$

$$H_1 = \frac{\hbar\Omega}{2}[e^{i(\omega t + \varphi)}S_- + e^{-i(\omega t + \varphi)}S_+], \quad (5)$$

$$H_2 = \hbar g(aS_+ + a^\dagger S_-). \quad (6)$$

The Hamiltonian (3), together with the Hamiltonians (4)–(6), can be implemented when the qubits are atoms [40,41], quantum dots, or superconducting devices (e.g., see Sec. V). Here,  $H_0$  is the free Hamiltonian of the qubits and the cavity mode,  $H_1$  is the interaction Hamiltonian between the qubits and the classical pulse, and  $H_2$  is the interaction Hamiltonian between the qubits and the cavity mode. In addition,  $\omega_0$  is the transition frequency between the two levels  $|0\rangle$  and  $|1\rangle$  of each qubit;  $a$  ( $a^\dagger$ ) is the photon annihilation (creation) operator of the cavity mode with frequency  $\omega_c$ ;  $g$  is the coupling constant between the cavity mode and each qubit;  $\Omega$ ,  $\omega$ , and  $\varphi$  are the Rabi frequency, the frequency, and the initial phase of the pulse, respectively; and  $S_z$ ,  $S_-$ , and  $S_+$  are the collective operators for the  $n + 1$  qubits, which are given by

$$S_z = \sum_{j=1}^{n+1} \sigma_{z,j}, \quad S_- = \sum_{j=1}^{n+1} \sigma_j^-, \quad S_+ = \sum_{j=1}^{n+1} \sigma_j^+, \quad (7)$$

where  $\sigma_{z,j} = |0_j\rangle\langle 0_j| - |1_j\rangle\langle 1_j|$ ,  $\sigma_j^- = |0_j\rangle\langle 1_j|$ , and  $\sigma_j^+ = |1_j\rangle\langle 0_j|$ , with  $|0_j\rangle$  and  $|1_j\rangle$  ( $j = 1, 2, \dots, n + 1$ ) being the ground state and excited level of the  $j$ th qubit. In the interaction picture with respect to  $H_0$ , these Hamiltonians  $H_1$  and  $H_2$  are rewritten, respectively, as (under the assumption that  $\omega = \omega_0$ )

$$H_1 = \frac{\hbar\Omega}{2}(e^{i\varphi}S_- + e^{-i\varphi}S_+), \quad (8)$$

$$H_2 = \hbar g(e^{i\delta t}aS_+ + e^{-i\delta t}a^\dagger S_-), \quad (9)$$

where

$$\delta = \omega_0 - \omega_c \quad (10)$$

is the detuning between the  $|0\rangle \leftrightarrow |1\rangle$  transition frequency  $\omega_0$  of each qubit and the frequency  $\omega_c$  of the cavity mode.

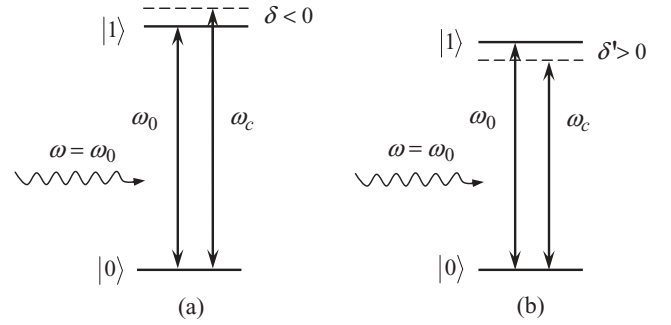


FIG. 2. Illustration of different detunings between the cavity mode frequency  $\omega_c$  and the qubit transition frequency  $\omega_0$ . Here,  $\omega_0$ ,  $\omega_c$ , and  $\omega$  are the qubit transition frequency, the cavity mode frequency, and the pulse frequency, respectively. In (a), the detuning is  $\delta = \omega_0 - \omega_c < 0$ . In (b), the detuning is  $\delta' = \omega_0 - \omega_c > 0$ . To implement an NTCP gate, we propose two alternative approaches (see Sec. IV), each one with three steps. The first step for either method requires a negative detuning ( $\delta < 0$ ), as shown in (a). For either method, the second step requires a positive detuning ( $\delta' > 0$ ), as shown in (b).

We now consider two special cases:  $\varphi = \pi$  and negative detuning  $\delta < 0$ , as well as  $\varphi = 0$  and positive detuning  $\delta > 0$ . The detailed discussion of these two cases will be given in the Secs. III A and III B. The results from the unitary evolution, obtained for these two special cases, will be employed by the two alternative approaches (presented in Sec. IV) for the gate implementation.

#### A. Case for pulse phase $\varphi = \pi$ and detuning $\delta < 0$

In this subsection, we consider the negative detuning case  $\delta < 0$  [Fig. 2(a)]. When  $\varphi = \pi$ , the Hamiltonian (8) reduces to

$$H_1 = -\frac{\hbar\Omega}{2}S_x, \quad (11)$$

where

$$S_x = S_- + S_+ = \sum_{j=1}^{n+1} \sigma_{x,j}, \quad (12)$$

with  $\sigma_{x,j} = \sigma_j^- + \sigma_j^+$ . Performing the unitary transformation  $|\psi(t)\rangle = e^{-iH_1 t}|\psi'(t)\rangle$ , we obtain

$$i\hbar \frac{d}{dt}|\psi'(t)\rangle = \overline{H}_2 |\psi'(t)\rangle, \quad (13)$$

with

$$\begin{aligned} \overline{H}_2 &= \exp[iH_1 t/\hbar] H_2 \exp[-iH_1 t/\hbar] \\ &= \frac{\hbar g}{2} \left\{ e^{i\delta t} a \left[ S_x + \frac{1}{2}(S_z - S_- + S_+) e^{-i\Omega t} \right. \right. \\ &\quad \left. \left. - \frac{1}{2}(S_z + S_- - S_+) e^{i\Omega t} \right] \right\} + \text{H.c.} \end{aligned} \quad (14)$$

Assuming that  $\Omega \gg |\delta|, g$ , we can neglect the fast-oscillating terms [40–42]. Then the Hamiltonian (14) reduces to [40–42]

$$\overline{H}_2 = \frac{\hbar g}{2}(e^{i\delta t} a + e^{-i\delta t} a^\dagger)S_x. \quad (15)$$

The evolution operator for the Hamiltonian (15) can be written in the form [19,40,43,44]

$$u(t) = e^{-iA(t)S_x^2} e^{-iB(t)S_x a} e^{-iB^*(t)S_x a^\dagger}, \quad (16)$$

where

$$\begin{aligned} B(t) &= \frac{g}{2} \int_0^t e^{i\delta t'} dt' = \frac{g}{2i\delta} (e^{i\delta t} - 1), \\ A(t) &= i \int_0^t B(t') \frac{dB^*(t')}{dt'} dt' \\ &= \frac{g^2}{4\delta} \left[ t + \frac{1}{i\delta} (e^{-i\delta t} - 1) \right]. \end{aligned} \quad (17)$$

When the evolution time  $t$  satisfies  $t = \tau = 2\pi/|\delta|$ , we have  $B(\tau) = 0$  and  $A(\tau) = g^2\tau/(4\delta)$ . Then we obtain

$$u(\tau) = \exp(i\lambda\tau S_x^2), \quad (18)$$

where  $\lambda = -g^2/(4\delta) > 0$ . The evolution operator of the system (in the interaction picture with respect to  $H_0$ ) is thus given by

$$U(\tau) = e^{-iH_1\tau/\hbar} u(\tau) = e^{i\Omega\tau S_x/2} e^{i\lambda\tau S_x^2}. \quad (19)$$

In Sec. IV, we propose two alternative approaches for the NTCP gate implementation, each one involving three steps. The evolution operator  $U$  in Eq. (19) will be needed for the first step for either one of the two alternative approaches.

### B. Case for pulse phase $\varphi = 0$ and detuning $\delta > 0$

In the following, we consider the positive detuning case,  $\delta > 0$ . The detuning  $\delta$  can be adjusted from  $\delta < 0$  to  $\delta > 0$  by changing either the qubit transition frequency  $\omega_0$  or the cavity mode frequency  $\omega_c$ , or both. In general, the qubit-cavity coupling constant varies when the detuning changes. To distinguish this case ( $\varphi = 0$  and  $\delta > 0$ ) from the previous case ( $\varphi = \pi$  and  $\delta < 0$ ), we replace the previous notation  $\Omega$ ,  $\delta$ , and  $g$  by  $\Omega'$ ,  $\delta'$ , and  $g'$ , respectively [see Fig. 2(b)]. For simplicity, we use the same symbols  $\omega$ ,  $\omega_0$ , and  $\omega_c$  for the pulse frequency, the qubit transition frequency, and the cavity mode frequency [Fig. 2(b)].

Suppose now that qubit 1 is largely detuned (decoupled) from both the cavity mode and the pulse. This can be achieved by adjusting the level spacing of qubit 1 (a tunability of energy levels that can be achieved in different types of qubits, e.g., solid-state qubits [30–34]), or by moving qubit 1 out of the cavity mode (e.g., trapped atoms [20,45,46]). Thus, after dropping the terms related to qubit 1 (i.e., the terms corresponding to the index  $j = 1$ ) from the collective operators  $S_+ = \sum_{j=1}^{n+1} \sigma_j^+$  and  $S_- = \sum_{j=1}^{n+1} \sigma_j^-$  in Hamiltonians (8) and (9), and replacing  $\Omega$ ,  $\delta$ , and  $g$  (for the case of  $\varphi = \pi$  and  $\delta < 0$ ) with  $\Omega'$ ,  $\delta'$ , and  $g'$  (for the case of  $\varphi = 0$  and  $\delta > 0$ ), we obtain from the Hamiltonians (8) and (9) (assuming  $\omega = \omega_0$ )

$$H'_1 = \frac{\hbar\Omega'}{2} (e^{i\varphi} S'_- + e^{-i\varphi} S'_+), \quad (20)$$

$$H'_2 = \hbar g' (e^{i\delta't} a S'_+ + e^{-i\delta't} a^\dagger S'_-), \quad (21)$$

which are written in the interaction picture with respect to  $H_0$  in Eq. (4). Here,  $S'_-$  and  $S'_+$  are the collective operators for the  $n$  qubits (2, 3, ...,  $n+1$ ), which are given by

$$S'_- = \sum_{j=2}^{n+1} \sigma_j^-, \quad S'_+ = \sum_{j=2}^{n+1} \sigma_j^+. \quad (22)$$

In addition, the detuning  $\delta'$  is

$$\delta' = \omega_0 - \omega_c > 0. \quad (23)$$

When choosing  $\varphi = 0$ , the Hamiltonian (20) reduces to

$$H'_1 = \frac{\hbar\Omega'}{2} S'_x, \quad (24)$$

where

$$S'_x = S'_- + S'_+ = \sum_{j=2}^{n+1} \sigma_{x,j}. \quad (25)$$

Note that the Hamiltonian (24) has a form similar to Eq. (11) and that the Hamiltonian (21) has a form similar to Eq. (9). Therefore, it is straightforward to show that under the condition  $\Omega' \gg \delta'$ ,  $g'$ , when  $t = \tau' = 2\pi/\delta'$ , the evolution operator of the qubits (in the interaction picture with respect to  $H_0$ ) is

$$U'(\tau') = \exp(-i\Omega'\tau' S'_x/2) \exp(-i\lambda'\tau' S_x'^2), \quad (26)$$

where  $\lambda' = g'^2/(4\delta') > 0$ . The evolution operator  $U'$  in Eq. (26) will be needed for the second step of either one of the two alternative approaches (presented in Sec. IV) for implementing the NTCP gate.

One can see that the operator described by Eq. (19) or Eq. (26) does not include the photon operator  $a$  or  $a^\dagger$  of the cavity mode. Therefore, the cavity mode can be initially in an arbitrary state (e.g., in a vacuum state, a Fock state, a coherent state, or even a thermal state).

For the gate realization, we will also need to have the qubits decoupled from the cavity mode and apply a resonant pulse to each qubit. Suppose that the Rabi frequency for the pulse applied to qubit 1 is  $\Omega_1$  while the Rabi frequency for the pulses applied to qubits 2, 3, ...,  $n+1$  is  $\Omega_r$ . The initial phase for each pulse is  $\varphi = 0$ . The free Hamiltonian of the qubits and the cavity mode is the  $H_0$  given in Eq. (4). In the interaction picture with respect to  $H_0$ , the interaction Hamiltonian for the qubit system and the pulses is given by

$$\tilde{H} = \frac{\hbar\Omega_1}{2} \sigma_{x,1} + \frac{\hbar\Omega_r}{2} S'_x. \quad (27)$$

For an evolution time  $\tau$ , the time evolution operator for the Hamiltonian (27) is

$$\tilde{U}(\tau) = \exp[-i\Omega_1\tau\sigma_{x,1}/2] \exp[-i\Omega_r\tau S'_x/2]. \quad (28)$$

The evolution operator  $\tilde{U}$  in Eq. (28) will be needed for the third step for either one of the two alternative approaches in the following.

## IV. IMPLEMENTATION OF THE NTCP GATE

The goal of this section is to demonstrate how the NTCP gate can be realized based on the unitary operators (19), (26), and (28) just obtained. We will present two alternative

methods for the gate implementation: one method based on the adjustment of the qubit transition frequency and another method which works mainly via the adjustment of the cavity mode frequency.

### A. NTCP gate via adjusting the qubit transition frequency

Let us consider  $n + 1$  qubits placed in a single-mode cavity or coupled to a resonator. For this first method, the cavity mode frequency  $\omega_c$  is kept fixed. The operations for the gate implementation and the unitary evolutions after each step of operation are as follows:

Step (i): Apply a resonant pulse (with  $\varphi = \pi$ ) to each qubit. The pulse Rabi frequency is  $\Omega$ . The cavity mode is coupled to each qubit with a detuning  $\delta < 0$  [Figs. 3(a) and 3(a')]. This is the case discussed in Sec. III A. Thus, the  $U$  in Eq. (19) is the evolution operator for the qubit system for an interaction time  $\tau = -2\pi/\delta$ .

Step (ii): Adjust the qubit transition frequency for qubits 2, 3, ...,  $n + 1$ , such that the cavity mode is coupled to qubits 2, 3, ...,  $n + 1$  with a detuning  $\delta' > 0$  [Fig. 3(b')]. Apply a resonant pulse (with  $\varphi = 0$ ) to each of the target qubits (2, 3, ...,  $n + 1$ ) [Fig. 3(b')]. The pulse Rabi frequency is now  $\Omega'$ . In addition, adjust the transition frequency of qubit 1 such that qubit 1 is decoupled from the cavity mode and the pulses applied to qubits 2, 3, ...,  $n + 1$  [Fig. 3(b)]. It can be seen that this is the case discussed in Sec. III B. Thus, the  $U'$  in Eq. (26) is the evolution operator for the qubit system for an interaction time  $\tau' = 2\pi/\delta'$ .

The combined time evolution operator, after these two steps, is

$$\begin{aligned} U(\tau + \tau') &= U'(\tau')U(\tau) \\ &= e^{-i\Omega'\tau'S'_x/2} e^{-i\lambda'\tau'S_x^2} e^{i\Omega\tau S_x/2} e^{i\lambda\tau S_x^2} \\ &= \exp[i\Omega\tau(S_x - S'_x)/2] \exp[i\lambda\tau(S_x^2 - S_x'^2)]. \end{aligned} \quad (29)$$

In the last line of Eq. (29), we assumed  $\Omega\tau = \Omega'\tau'$  (i.e.,  $-\Omega/\delta = \Omega'/\delta'$ ) and  $\lambda\tau = \lambda'\tau'$  (i.e.,  $-g/\delta = g'/\delta'$ ), which can be achieved by adjusting the detunings  $\delta$  and  $\delta'$  (i.e., changing the qubit transition frequency) as well as the Rabi frequencies  $\Omega$  and  $\Omega'$  (i.e., changing the intensity of the pulses). Note that  $S_x - S'_x = \sigma_{x,1}$  and  $S_x^2 - S_x'^2 = I + 2\sigma_{x,1}S'_x$ , where  $I$  is the identity operator for qubit 1. Thus, Eq. (29) can be written as

$$U(\tau + \tau') = \exp[i\Omega\tau\sigma_{x,1}/2] \exp[i2\lambda\tau\sigma_{x,1}S'_x]. \quad (30)$$

Step (iii): Leave the transition frequency unchanged for qubit 1 [Fig. 3(c)] but adjust the transition frequency of qubits 2, 3, ...,  $n + 1$  [Fig. 3(c')], such that the cavity mode is largely detuned (decoupled) from each qubit. In addition, apply a resonant pulse (with  $\varphi = 0$ ) to each qubit. The Rabi frequency for the pulse applied to qubit 1 is now  $\Omega_1$  [Fig. 3(c)] while the Rabi frequency of the pulse applied to qubits 2, 3, ...,  $n + 1$  is  $\Omega_r$  [Fig. 3(c')]. In this case, the interaction Hamiltonian for the qubit system and the pulses is given by Eq. (27) and thus the time evolution operator is the  $\tilde{U}$  in Eq. (28) for an evolution time  $\tau$  given in step (i) above.

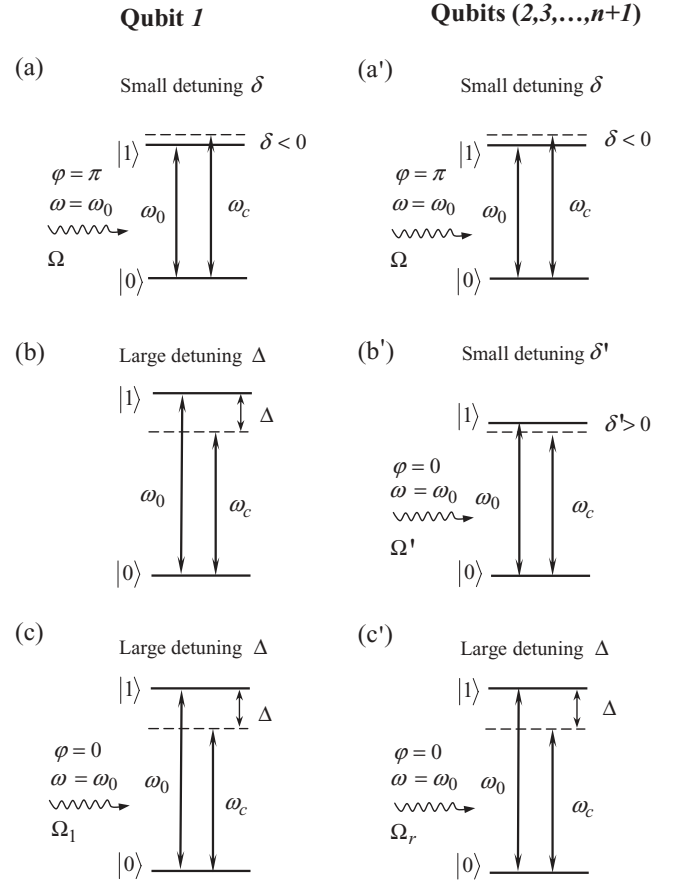


FIG. 3. Change of the qubit transition frequency  $\omega_0$  (or the qubit level spacings) of each qubit during a three-step NTCP gate. The three figures on the left side correspond to the control qubit 1 while the three figures on the right side correspond to each of the target qubits (2, 3, ...,  $n + 1$ ). Figures (a) and (a'), figures (b) and (b'), and figures (c) and (c') correspond to the operations of step (i), step (ii), and step (iii), respectively. In each figure, the two horizontal solid lines represent the qubit energy levels for the states  $|0\rangle$  and  $|1\rangle$ ;  $\omega_0$  is the qubit  $|0\rangle \leftrightarrow |1\rangle$  transition frequency;  $\omega_c$  is the cavity mode frequency;  $\omega$  is the pulse frequency;  $\varphi$  is the initial phase of the pulse; and  $\Omega$ ,  $\Omega'$ ,  $\Omega_1$ , and  $\Omega_r$  are the Rabi frequencies of various applied pulses. In addition,  $\delta$  and  $\delta'$  are the small detunings of the cavity mode with the  $|0\rangle \leftrightarrow |1\rangle$  transition, which are given by  $\delta = \omega_0 - \omega_c < 0$  and  $\delta' = \omega_0 - \omega_c > 0$ ;  $\Delta = \omega_0 - \omega_c$  represents the large detuning of the cavity mode with the  $|0\rangle \leftrightarrow |1\rangle$  transition. Note that the cavity mode frequency  $\omega_c$  is kept fixed during the entire process, but the qubit transition frequency  $\omega_0$  is adjusted to achieve a different detuning  $\delta, \delta'$ , or  $\Delta$  for each step.

It can be seen that after this three-step operation, the joint time-evolution operator of the qubit system is

$$\begin{aligned} U(2\tau + \tau') &= \tilde{U}(\tau)U(\tau + \tau') \\ &= e^{-i(\Omega_1 - \Omega)\tau\sigma_{x,1}/2} e^{-i\Omega_r\tau S'_x/2} e^{i2\lambda\tau\sigma_{x,1}S'_x}. \end{aligned} \quad (31)$$

Under the conditions

$$\begin{aligned} \Omega_1 &= 4\lambda n + \Omega = -ng^2/\delta + \Omega, \\ \Omega_r &= 4\lambda = -g^2/\delta \end{aligned} \quad (32)$$

(which can be obtained by adjusting the Rabi frequencies  $\Omega$ ,  $\Omega_1$  and  $\Omega_r$ ), Eq. (31) can be then written as

$$U(2\tau + \tau') = \prod_{j=2}^{n+1} U_p(1, j), \quad (33)$$

with

$$U_p(1, j) = \exp[-i2\lambda\tau(\sigma_{x,1} + \sigma_{x,j} - \sigma_{x,1}\sigma_{x,j})]. \quad (34)$$

It can be easily shown that for the qubit pair  $(1, j)$ , we have

$$\begin{aligned} U_p(1, j)|+1\rangle|+j\rangle &= |+1\rangle|+j\rangle, \\ U_p(1, j)|+1\rangle|-j\rangle &= |+1\rangle|-j\rangle, \\ U_p(1, j)|-1\rangle|+j\rangle &= |-1\rangle|+j\rangle, \\ U_p(1, j)|-1\rangle|-j\rangle &= \exp(i8\lambda\tau)|-1\rangle|-j\rangle, \end{aligned} \quad (35)$$

where an overall phase factor  $\exp(-i2\lambda\tau)$  is omitted. Here and in the following,  $|+1\rangle = (|0_1\rangle + |1_1\rangle)/\sqrt{2}$  and  $|-1\rangle = (|0_1\rangle - |1_1\rangle)/\sqrt{2}$  are the two eigenstates of the Pauli operator  $\sigma_{x,1}$  for qubit 1, while  $|+j\rangle = (|0_j\rangle + |1_j\rangle)/\sqrt{2}$  and  $|-j\rangle = (|0_j\rangle - |1_j\rangle)/\sqrt{2}$  are the two eigenstates of the Pauli operator  $\sigma_{x,j}$  for qubit  $j$  ( $j = 2, 3, \dots, \text{or } n+1$ ). By setting  $8\lambda\tau = (2k+1)\pi$ , that is,

$$4g^2/\delta^2 = 2k+1 \quad (36)$$

(where  $k$  is an integer), we obtain from Eq. (35)

$$\begin{aligned} U_p(1, j)|+1\rangle|+j\rangle &= |+1\rangle|+j\rangle, \\ U_p(1, j)|+1\rangle|-j\rangle &= |+1\rangle|-j\rangle, \\ U_p(1, j)|-1\rangle|+j\rangle &= |-1\rangle|+j\rangle, \\ U_p(1, j)|-1\rangle|-j\rangle &= -|-1\rangle|-j\rangle, \end{aligned} \quad (37)$$

which shows that a quantum phase gate described by

$$U_p(1, j) = I_j - 2|-1\rangle\langle -1| \quad (38)$$

is achieved for the qubit pair  $(1, j)$ . Here,  $I_j$  is the identity operator for the qubit pair  $(1, j)$ , which is given by  $I_j = \sum_{kl} |k_1 l_j\rangle\langle k_1 l_j|$  with  $k, l \in \{+, -\}$ . Note that the condition (36) can be achieved by adjusting the detuning  $\delta$  (i.e., via changing the qubit transition frequency  $\omega_0$ ).

Combining Eqs. (33) and (38), we finally obtain

$$U(2\tau + \tau') = \prod_{j=2}^{n+1} (I_j - 2|-1\rangle\langle -1|), \quad (39)$$

which demonstrates that  $n$  two-qubit CP gates are simultaneously performed on the qubit pairs  $(1, 2)$ ,  $(1, 3)$ ,  $\dots$ , and  $(1, n+1)$ , respectively. Note that each qubit pair contains the same control qubit (qubit 1) and a different target qubit (qubit 2, 3,  $\dots$ , or  $n+1$ ). Hence, an NTCP gate with  $n$  target qubits  $(2, 3, \dots, n+1)$  and one control qubit (qubit 1) is obtained after this three-step process.

From this description, one can see that the method presented here has an advantage: It does not require the adjustment of the cavity-mode frequency.

## B. NTCP gate via mainly adjusting the cavity-mode frequency

In this subsection, we present a different way for realizing the NTCP gate, which is mainly based on the adjustment of the cavity mode frequency  $\omega_c$ .

Let us consider  $n+1$  qubits placed in a single-mode cavity or coupled to a resonator. Note that now the transition frequency  $\omega_0$  of the  $n$  target qubits  $(2, 3, \dots, n+1)$  is kept fixed during the following entire process. The operations for the gate implementation and the unitary evolutions after each step are as follows:

Step (i): Apply a resonant pulse (with  $\varphi = \pi$ ) to each qubit. The pulse Rabi frequency is  $\Omega$ . The cavity mode is coupled to each qubit with a detuning  $\delta < 0$  [Figs. 4(a) and 4(a')]. It can be seen that this is the case discussed in Sec. III A. Thus, the  $U$  in Eq. (19) is the evolution operator for the qubit system for an interaction time  $\tau = -2\pi/\delta$ .

Step (ii): Leave the transition frequency  $\omega_0$  of qubits  $2, 3, \dots, n+1$  unchanged while adjusting the cavity mode frequency  $\omega_c$ . The cavity mode is coupled to qubits  $2, 3, \dots, n+1$  with a detuning  $\delta' > 0$  [Fig. 4(b')]. Apply a resonant pulse (with  $\varphi = 0$ ) to each of qubits  $2, 3, \dots, n+1$  [Fig. 4(b')]. The pulse Rabi frequency is now  $\Omega'$ . In addition, adjust the transition frequency of qubit 1, such that qubit 1 is largely detuned (decoupled) from the cavity mode as well as the pulses applied to qubits  $2, 3, \dots, n+1$  [Fig. 4(b)]. One can see that this is the case discussed in Sec. III B. Hence, the  $U'$  in Eq. (26) is the evolution operator for the qubit system for an interaction time  $\tau' = 2\pi/\delta'$ .

Step (iii): Leave the transition frequency  $\omega_0$  of qubits  $2, 3, \dots, n+1$  unchanged while adjusting the transition frequency of the control qubit 1 back to its original setting in step (i) [Fig. 4(c)]. Adjust the cavity mode frequency  $\omega_c$ , such that the cavity mode is largely detuned (decoupled) from each qubit [Figs. 4(c) and 4(c')]. In addition, apply a resonant pulse (with  $\varphi = 0$ ) to each qubit. The Rabi frequency for the pulse applied to qubit 1 is now  $\Omega_1$  [Fig. 4(c)] while the Rabi frequency of the pulses applied to qubits  $2, 3, \dots, n+1$  is now  $\Omega_r$  [Fig. 4(c')]. Therefore, the interaction Hamiltonian for the qubits and the pulses is  $H_1$  in Eq. (27) and thus the time evolution operator is the  $\tilde{U}$  in Eq. (28) for the evolution time  $\tau$  given in step (i) above.

Note that the time evolution operators  $U$ ,  $U'$ , and  $\tilde{U}$ , obtained from each step discussed in this section, are the same as those obtained from each step of operations in the previous section. Hence, it is clear that the NTCP gate can be implemented after this three-step process.

From this description, it can be seen that the transition frequency  $\omega_0$  for each one of the  $n$  target qubits  $(2, 3, \dots, n+1)$  remains unchanged during the entire operation. Thus, adjusting the level spacings for the  $n$  target qubits  $(2, 3, \dots, n+1)$  is not required by the method presented in this section. What one needs to do is to adjust the cavity mode frequency and the level spacings of the control qubit 1.

## C. Discussion

We have presented two alternative methods for implementing an NTCP gate. Note that when coupled to a cavity (or resonator) mode and driven by a classical pulse, physical qubit systems (such as atoms, quantum dots, and superconducting

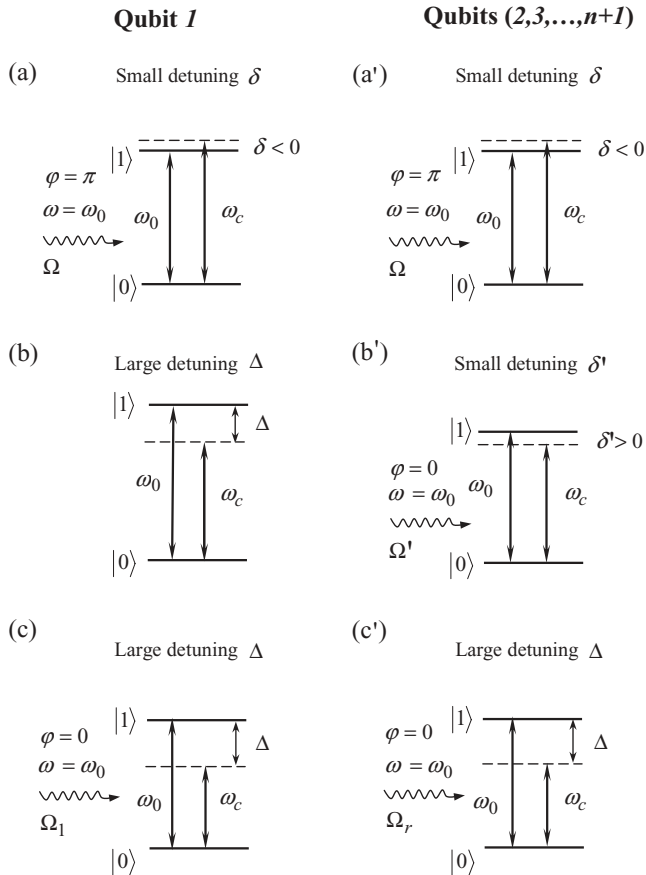


FIG. 4. Change of the cavity mode frequency  $\omega_c$  and the transition frequency  $\omega_0$  (or the level spacings) of qubit 1 during a three-step NTCP gate. This second method is an alternative way to implement the NTCP gate, which is different from the steps shown in Fig. 3. Note that the transition frequency  $\omega_0$  for qubits  $2, 3, \dots, n+1$  remains unchanged during this method. The three figures on the left side correspond to the control qubit 1, which (from top to bottom) are for the operations of step (i), step (ii), and step (iii), respectively. The three figures on the right side correspond to each of the qubits  $2, 3, \dots, n+1$ , which (from top to bottom) are, respectively, for the operations of step (i), step (ii), and step (iii). In each figure, the two horizontal solid lines represent the qubit levels  $|0\rangle$  and  $|1\rangle$ ;  $\omega_0$  is the qubit transition frequency;  $\omega_c$  is the cavity mode frequency;  $\omega$  is the pulse frequency;  $\varphi$  is the initial phase of the pulse; and  $\Omega$ ,  $\Omega'$ ,  $\Omega_1$ , and  $\Omega_r$  are the Rabi frequencies of the pulses (for various steps). In addition,  $\delta$  and  $\delta'$  are the small detunings of the cavity mode with the  $|0\rangle \leftrightarrow |1\rangle$  transition, which are given by  $\delta = \omega_0 - \omega_c < 0$  and  $\delta' = \omega_0 - \omega_c > 0$ ;  $\Delta = \omega_0 - \omega_c$  represents the large detuning of the cavity mode with the  $|0\rangle \leftrightarrow |1\rangle$  transition.

qubits) have the same type of interaction described by the Hamiltonian (3) or a Hamiltonian having a similar form to Eq. (3), from which the four Hamiltonians (8), (9), (20), and (21) (i.e., the key elements for the proposed NTCP gate implementation) are available. Therefore, the two alternative methods here are quite general, which can be applied to implementing the NTCP gate with superconducting qubits, quantum dots, or trapped atomic qubits.

As shown, the first method is based on the adjustment of the qubit level spacings while the second method works mainly via the adjustment of the cavity mode frequency. For solid-

state qubits, the qubit level spacings can be rapidly adjusted (e.g., in 1–2 ns time scale for superconducting qubits [47]). And, for superconducting resonators, the resonator frequency can be fast tuned (e.g., in less than a few nanoseconds for a superconducting transmission line resonator [36]).

In the Appendix, we provide guidelines on protecting qubits from leaking out of the computational subspace in the presence of more qubit levels. As discussed there, as long as the large detuning of the cavity mode with the transition between the irrelevant energy levels can be met, the leakage out of the computational subspace induced by the cavity mode can be suppressed. In addition, we should mention that since the applied pulses are *resonant* with the  $|0\rangle \leftrightarrow |1\rangle$  transition, the coupling of the qubit level  $|0\rangle$  or  $|1\rangle$  with other levels, induced by the pulses, is negligibly small. Therefore, the leak out of the computation subspace, due to the application of the pulses, can be neglected.

As discussed earlier, during the gate operation for either of the two methods, decoupling of the qubits from the cavity was made by adjusting the qubit frequency  $\omega_0$  or the cavity frequency  $\omega_c$ . This particularly applies to solid-state qubits because the locations of solid-state qubits (such as superconducting qubits and quantum dots) are fixed once they are built in a cavity or resonator. However, it is noted that for trapped atomic qubits, decoupling of qubits from the cavity can be made by just moving atoms out of the cavity and thus adjustment of the level spacings of atoms or the cavity frequency is not needed to have atoms decoupled (largely detuned) from the cavity mode (e.g., as shown in Sec. VI).

For both step (i) and step (ii) of the two methods here, it was assumed that the detuning  $\delta$  ( $\delta'$ ) is much smaller than the qubit Rabi frequency  $\Omega$  ( $\Omega'$ ) and that the Rabi frequencies are equal for all the qubits. In reality, the Rabi frequency for each qubit might not be identical, and the effect of the small Rabi frequency deviations on the gate performance may be magnified when the operation time is much longer than the inverse Rabi frequency. Hence, to improve the gate performance, the Rabi frequency deviations should be as small as possible, which could be achieved by adjusting the intensity of the pulses applied to the qubits.

We should mention that when the mean photon number  $\bar{n}$  of the cavity field satisfies  $\bar{n} \leq 1$ , the multiphoton process can be neglected. In the case when the condition  $\bar{n} \leq 1$  is not met, one can adjust the qubit level spacings or choose the qubit level structures appropriately, such that the multiphoton process is negligible during the quantum operation.

Before closing this section, it should be mentioned that the present method is based on an effective Hamiltonian

$$H_{\text{eff}} = \sum_{j=2}^{n+1} H_{1j} = 2\hbar\lambda \sum_{j=2}^{n+1} (\sigma_{x,1} + \sigma_{x,j} - \sigma_{x,1}\sigma_{x,j}), \quad (40)$$

which can be found from Eqs. (33) and (34). One can see that this Hamiltonian contains the interaction terms between the control qubit (qubit 1) and each target qubit, but it does not include the interaction terms between any two target qubits. Note that each term  $H_{1j}$  in Eq. (40) acts on a different target qubit, with the same control qubit, and that any two terms  $H_{1j}$  for different  $j$ 's commute with each other. Therefore, the  $n$  two-qubit controlled-phase gates forming the NTCP gate

can be *simultaneously* performed on the qubit pairs (1,2), (1,3), . . . , and (1,  $n + 1$ ), respectively.

## V. REALIZING THE NTCP GATE WITH SUPERCONDUCTING QUBITS COUPLED TO A RESONATOR

The methods presented so far for implementing the NTCP gate are based on the four Hamiltonians (8), (9), (20) and (21). In this section, we show how these Hamiltonians can be obtained for the superconducting charge qubits coupled to a resonator. We will then show how to apply the first method to implement the NTCP gate with  $n + 1$  charge qubits selected from  $N$  charge qubits coupled to a resonator ( $1 < n < N$ ). A discussion on the experimental feasibility will be given later.

### A. Hamiltonians

The superconducting charge qubit considered here, as shown in Fig. 5(a), consists of a small superconducting box with excess Cooper-pair charges, connected to a symmetric superconducting quantum interference device (SQUID) with capacitance  $C_{J0}$  and Josephson coupling energy  $E_{J0}$ . In the charge regime  $\Delta \gg E_c \gg E_{J0} \gg k_B T$  (where,  $k_B$ ,  $\Delta$ ,  $E_c$ , and  $T$  are the Boltzmann constant, superconducting energy gap, charging energy, and temperature, respectively), only two charge states,  $n = 0$  and  $n = 1$ , are important for the dynamics of the system, and thus this device (e.g., [30–32]) behaves as a two-level system. Here, we denote the two charge states  $n = 0$  and  $n = 1$  as the two eigenstates  $|+\rangle$  and  $|-\rangle$  of the spin

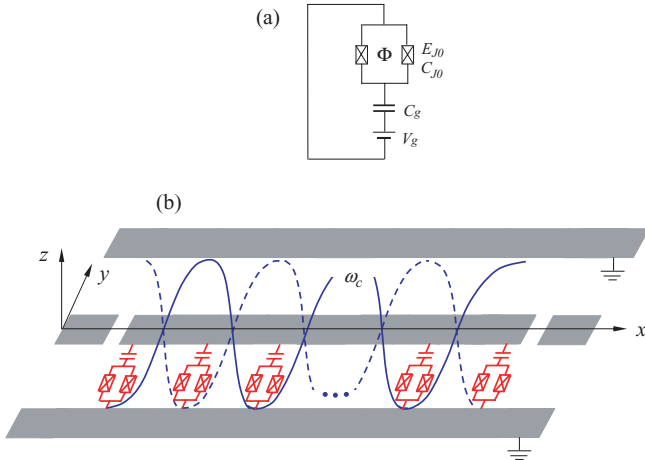


FIG. 5. (Color online) (a) Schematic diagram of a superconducting charge qubit. Here,  $E_{J0}$  is the Josephson coupling energy,  $C_{J0}$  is the Josephson capacitance,  $C_g$  is the gate capacitance,  $V_g$  is the gate voltage, and  $\Phi$  is the external magnetic flux applied to the SQUID loop through a control line (not shown). (b)  $N$  superconducting qubits are placed into a (gray) quasi-one-dimensional transmission line resonator. Each qubit is placed at an antinode of the electric field, yielding a strong coupling between the qubit and the resonator mode. The two blue curves represent the standing-wave electric field, along the  $y$  direction. A subset of qubits from the  $N$  qubits, selected for the gate, are coupled to each other via the resonator mode, while the remaining qubits, which are not controlled by the gate, are decoupled from the resonator mode by setting their  $\Phi = \Phi_0/2$ ,  $V_g^{dc} = e/C_g$ , and  $V_g^{ac} = 0$  to have their free Hamiltonian equal to zero.

operator  $\tilde{\sigma}_z$ . The reason for not using the eigenstates  $|0\rangle$  and  $|1\rangle$  of  $\sigma_z$  to represent the two charge states is that in order to obtain the four Hamiltonians (8), (9), (20), and (21), in the following we will need to perform a basis transformation from the  $\tilde{\sigma}_z$  basis  $\{|+\rangle, |-\rangle\}$  to the  $\sigma_z$  basis  $\{|0\rangle, |1\rangle\}$ . The Hamiltonian describing the qubit is given by [30,31]

$$H_q = -2E_c(1 - 2n_g)\tilde{\sigma}_z - E_J(\Phi)\tilde{\sigma}_x, \quad (41)$$

where  $n_g = C_g V_g / (2e)$ ,  $E_c = e^2 / (2C_g + 4C_{J0})$ ,  $E_J(\Phi) = 2E_{J0} \cos(\pi \Phi / \Phi_0)$ ,  $\tilde{\sigma}_z = |+\rangle\langle +| - |-\rangle\langle -|$ , and  $\tilde{\sigma}_x = |+\rangle\langle -| + |-\rangle\langle +|$ . Here,  $C_g$  is the gate capacitance,  $V_g$  is the gate voltage,  $\Phi$  is the external magnetic flux applied to the SQUID loop,  $\Phi_0 = h/2e$  is the flux quantum, and  $E_J(\Phi)$  is the effective Josephson coupling energy. We assume that  $V_g = V_g^{dc} + V_g^{ac} + V_g^{qu}$ , where  $V_g^{dc}$  ( $V_g^{ac}$ ) is the dc (ac) part of the gate voltage and  $V_g^{qu}$  is the quantum part of the gate voltage, which is caused by the electric field of the resonator mode when the qubit is coupled to a resonator. Correspondingly, we have

$$n_g = n_g^{dc} + n_g^{ac} + n_g^{qu}, \quad (42)$$

where  $n_g^{dc} = C_g V_g^{dc} / (2e)$ ,  $n_g^{ac} = C_g V_g^{ac} / (2e)$ , and  $n_g^{qu} = C_g V_g^{qu} / (2e)$ . By inserting Eq. (42) into Eq. (41), we obtain the following Hamiltonian for the qubit-cavity system:

$$H = E_z \tilde{\sigma}_z - E_J(\Phi) \tilde{\sigma}_x + \hbar \omega_c a^\dagger a + 4E_c n_g^{ac} \tilde{\sigma}_z + 4E_c n_g^{qu} \tilde{\sigma}_z, \quad (43)$$

where  $E_z = -2E_c(1 - 2n_g^{dc})$ . When  $V_g^{ac} = V_0 \cos(\omega t + \varphi)$  and  $V_g^{qu} = V_0^{qu}(a + a^\dagger)$ , the Hamiltonian (43) becomes [11,48]

$$H = E_z \tilde{\sigma}_z - E_J(\Phi) \tilde{\sigma}_x + \hbar \omega_c a^\dagger a + \hbar \Omega \cos(\omega t + \varphi) \tilde{\sigma}_z + \hbar g(a + a^\dagger) \tilde{\sigma}_z, \quad (44)$$

where  $\Omega = 2E_c C_g V_0 / (\hbar e)$  is the Rabi frequency of the ac gate voltage and  $g = 2E_c C_g V_0^{qu} / (\hbar e)$  is the coupling constant between the charge qubit and the resonator mode.

Let us now consider  $N$  identical charge qubits coupled to a single-mode resonator [Fig. 5(b)]. One can select a subset of qubits for the gate, while the remaining qubits, which are not controlled by the gate, are decoupled from the resonator mode by setting their  $\Phi = \Phi_0/2$ ,  $V_g^{dc} = e/C_g$ , and  $V_g^{ac} = 0$  to have their free Hamiltonian equal to zero. Without loss of generality, we assume that the set of qubits selected for the gate are the  $n + 1$  qubits labeled by 1, 2, . . . , and  $n + 1$  (where  $1 < n < N$ ). From our earlier discussion, it can be seen that the Hamiltonian for the  $n + 1$  qubits and the resonator mode is

$$H = E_z \tilde{S}_z - E_J(\Phi) \tilde{S}_x + \hbar \omega_c a^\dagger a + \hbar \Omega \cos(\omega t + \varphi) \tilde{S}_z + \hbar g(a + a^\dagger) \tilde{S}_z, \quad (45)$$

where  $\tilde{S}_z = \sum_{j=1}^{n+1} \tilde{\sigma}_{z,j}$  and  $\tilde{S}_x = \sum_{j=1}^{n+1} \tilde{\sigma}_{x,j}$ , with  $\tilde{\sigma}_{z,j} = |+_j\rangle\langle +_j| - |-_j\rangle\langle -_j|$  and  $\tilde{\sigma}_{x,j} = |+_j\rangle\langle -_j| + |-_j\rangle\langle +_j|$ . By setting  $E_z = 0$  (i.e.,  $n_g^{dc} = 1/2$ ) for each qubit and defining  $\omega_0/2 = E_J(\Phi)/\hbar$ , the Hamiltonian (45) reduces to

$$H = -\frac{\hbar \omega_0}{2} \tilde{S}_x + \hbar \omega_c a^\dagger a + \hbar \Omega \cos(\omega t + \varphi) \tilde{S}_z + \hbar g(a + a^\dagger) \tilde{S}_z. \quad (46)$$

Define now the new qubit basis  $|0_j\rangle = (|+_j\rangle + |-_j\rangle)/\sqrt{2}$  and  $|1_j\rangle = (|+_j\rangle - |-_j\rangle)/\sqrt{2}$ ; that is, perform a basis transformation from the  $\tilde{\sigma}_{z,j}$  basis  $\{|+_j\rangle, |-_j\rangle\}$  to the  $\sigma_{z,j}$  basis  $\{|0_j\rangle, |1_j\rangle\}$  for the  $j$ th qubit. Thus, in the new basis, the Hamiltonian (46) becomes

$$H = H_0 + H_1 + H_2, \quad (47)$$

where

$$H_0 = -\frac{\hbar\omega_0}{2}S_z + \hbar\omega_c a^\dagger a, \quad (48)$$

$$H_1 = \hbar\Omega \cos(\omega t + \varphi)S_x, \quad (49)$$

$$H_2 = \hbar g(a + a^\dagger)S_x. \quad (50)$$

Here, the collective operators  $S_z$  and  $S_x$  are the same as those given in Eqs. (7) and (12). In the interaction picture with respect to  $H_0$ , we obtain from Eqs. (49) and (50) (under the rotating-wave approximation and assuming  $\omega = \omega_0$ )

$$H_1 = \frac{\hbar\Omega}{2}(e^{i\varphi}S_- + e^{-i\varphi}S_+), \quad (51)$$

$$H_2 = \hbar g(e^{i\delta t}aS_+ + e^{-i\delta t}a^\dagger S_-), \quad (52)$$

where the collective operators  $S_-$  and  $S_+$  are the same as those given in Eq. (7), and  $\delta = \omega_0 - \omega_c < 0$ .

Note that  $\omega_0 = 4E_{J0} \cos(\pi\Phi/\Phi_0)/\hbar$ . Hence, the qubit transition frequency  $\omega_0$  can be adjusted by changing the external magnetic flux  $\Phi$  applied to the SQUID loop of the charge qubit.

We now turn off the ac gate voltage applied to the charge qubit 1 (i.e., setting  $V_g^{\text{ac}} = 0$  for the charge qubit 1) and adjust the transition frequency  $\omega_0$  of the charge qubit 1 to have qubit 1 decoupled (largely detuned) from the resonator mode. In this way, we can drop the terms corresponding to the index  $j = 1$  from the collective operators  $S_+ = \sum_{j=1}^{n+1} \sigma_j^+$  and  $S_- = \sum_{j=1}^{n+1} \sigma_j^-$  involved in Hamiltonians (51) and (52). In addition, adjust either the transition frequency  $\omega_0$  of qubits 2, 3, ...,  $n + 1$  or the resonator frequency  $\omega_c$ , to achieve a detuning  $\delta' = \omega_0 - \omega_c > 0$ , and set an ac gate voltage  $V_g^{\text{ac}} = V'_0 \cos(\omega t + \varphi)$  (with  $\omega = \omega_0$ ) for each of qubits 2, 3, ...,  $n + 1$ . The Rabi frequency  $\Omega'$  for each ac gate voltage (i.e., the pulse) is given by  $\Omega' = 2E_c C_g V'_0 / (\hbar e)$ . After replacing  $\Omega$ ,  $\delta$ , and  $g$ , with  $\Omega'$ ,  $\delta'$ , and  $g'$ , respectively, we can obtain from Eqs. (51) and (52)

$$H'_1 = \frac{\hbar\Omega'}{2}(e^{i\varphi}S'_- + e^{-i\varphi}S'_+), \quad (53)$$

$$H'_2 = \hbar g'(e^{i\delta' t}aS'_+ + e^{-i\delta' t}a^\dagger S'_-), \quad (54)$$

which are written in the interaction picture with respect to  $H_0$  in Eq. (48). Here, the collective operators  $S'_-$  and  $S'_+$  are the same as those given in Eq. (22).

One can see that the four Hamiltonians (51)–(54) obtained here have the same forms as the Hamiltonians (8), (9), (20), and (21), respectively. Hence, the NTCP gate can be implemented with charge qubits coupled to a resonator. A more detailed discussion on this is given in the next subsection.

### B. NTCP gates with charge qubits coupled to a resonator

Following the first method introduced in the previous section (see Sec. IV A), we now discuss how to implement

the NTCP gate with  $n + 1$  charge qubits (1, 2, ...,  $n + 1$ ), coupled to a superconducting resonator. To begin, it should be mentioned that (a) for each step of the operations, the dc gate voltage  $V_g^{\text{dc}}$  for each one of qubits 1, 2, ...,  $n + 1$  is set by  $V_g^{\text{dc}} = e/C_g$ , such that  $E_z = 0$  for each qubit, and (b) the resonator mode frequency  $\omega_c$  is fixed during the entire operation. The three-step operations for the gate realization are illustrated in Fig. 6.

From Fig. 6, it can be seen that there is no need for adjusting the resonator mode frequency  $\omega_c$ . Hence, the procedure here for the gate realization is an extension of the first method already introduced. Note that the three time-evolution

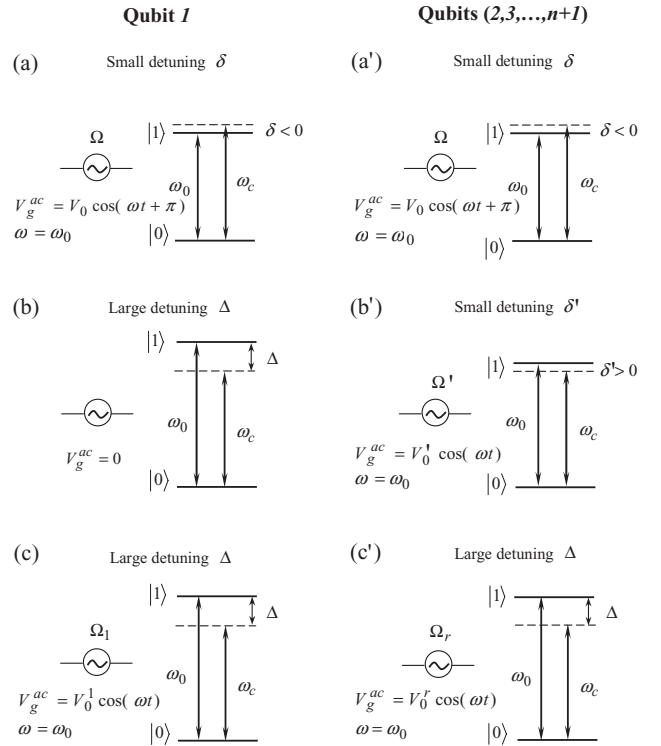


FIG. 6. Change of the qubit transition frequency  $\omega_0$  and the ac gate-voltage frequency  $\omega$  during a three-step NTCP gate with charge qubits coupled to a resonator. The three figures on the left side correspond to the charge control qubit 1, which (from top to bottom) are for the operations of step (i), step (ii), and step (iii), respectively. The three figures on the right side correspond to the charge target qubits (2, 3, ...,  $n + 1$ ) (from top to bottom) for the operations of step (i), step (ii), and step (iii), respectively. In each figure, the two horizontal solid lines represent the qubit levels  $|0\rangle$  and  $|1\rangle$ ;  $\omega_c$  is the resonator mode frequency;  $\omega_0$  is the qubit transition frequency;  $\omega$  is the frequency of the ac gate voltage  $V_g^{\text{ac}}$  (i.e., the pulse);  $\Omega(V_0)$ ,  $\Omega'(V_0')$ ,  $\Omega_1(V_0^1)$ , or  $\Omega_r(V_0^r)$  is a function of the amplitude  $V_0$ ,  $V_0'$ ,  $V_0^1$ , or  $V_0^r$  of the ac gate voltage, which can be adjusted by changing the ac gate-voltage amplitude; and each circle  $\sim$  represents an ac gate voltage. In (b), the ac gate voltage for qubit 1 is set to zero (i.e.,  $V_g^{\text{ac}} = 0$ ). In addition,  $\delta$  and  $\delta'$  are the small detunings of the resonator mode with the  $|0\rangle \leftrightarrow |1\rangle$  transition, which are given by  $\delta = \omega_0 - \omega_c < 0$  and  $\delta' = \omega_0 - \omega_c > 0$ ;  $\Delta = \omega_0 - \omega_c$  represents the large detuning of the resonator mode with the  $|0\rangle \leftrightarrow |1\rangle$  transition. Note that the resonator mode frequency  $\omega_c$  is kept fixed during the entire operation, but the qubit transition frequency  $\omega_0$  is adjusted to achieve a different detuning  $\delta, \delta'$ , or  $\Delta$  for each step.

operators  $U$ ,  $U'$ , and  $\tilde{U}$ , obtained from each step, are the same as those obtained from each step in Sec. IV A. Therefore, following the same discussion given there, one can easily see that the NTCP gate can be implemented with  $n + 1$  charge qubits (i.e., the control charge qubit 1, as well as the  $n$  target charge qubits 2, 3,  $\dots$ , and  $n + 1$ ). Namely, after the three-step process in Fig. 6, a phase flip (i.e.,  $|-\rangle \rightarrow -|-\rangle$ ) on the state  $|-\rangle$  of each target charge qubit is achieved when the control charge qubit 1 is initially in the state  $|-\rangle$ , but nothing happens to the states  $|+\rangle$  and  $|-\rangle$  of each target charge qubit when the control charge qubit 1 is initially in the state  $|+\rangle$ .

From the description above one can see that the spin operator  $\tilde{\sigma}_z$  is identical to  $\sigma_x$ . In other words, the states  $|+\rangle$  and  $|-\rangle$  are the eigenstates of both operators  $\tilde{\sigma}_z$  and  $\sigma_x$ . Thus, the NTCP gate (implemented with charge qubits here) is actually performed with respect to the eigenstates  $|+\rangle$  and  $|-\rangle$  of the spin operator  $\tilde{\sigma}_z$  (i.e., the two charge states  $n = 0$  and  $n = 1$  above, for each qubit).

According to the discussion in Sec. IV A, it can be found that to implement the NTCP gate, the following conditions need to be satisfied: (a)  $\Omega \gg g, \delta$  and  $\Omega' \gg g', \delta'$ ; (b)  $\Omega_1 = -ng^2/\delta + \Omega$  and  $\Omega_r = -g^2/\delta$ ; (c)  $-\Omega/\delta = \Omega'/\delta'$  and  $-g/\delta = g'/\delta'$ ; and (d)  $4g^2/\delta^2 = 2k + 1$ . These conditions can in principle be realized because (i) the Rabi frequencies  $\Omega(V_0)$ ,  $\Omega'(V'_0)$ ,  $\Omega_1(V_0^1)$ , and  $\Omega_r(V_0^r)$  are, respectively, functions of the amplitudes  $V_0$ ,  $V'_0$ ,  $V_0^1$ , and  $V_0^r$  of the ac gate voltages, which can be adjusted by changing the amplitudes of the ac gate voltages, and (ii) the detunings  $\delta$  and  $\delta'$  can be adjusted by changing the qubit transition frequency  $\omega_0$ .

Note that  $n_g^{\text{dc}} = 1/2$  (i.e.,  $E_z = 0$ ) was set for each qubit during the entire operation. We now give some discussion on the deviation from the degeneracy point  $n_g^{\text{dc}} = 1/2$  for each one of the qubits 1, 2,  $\dots$ ,  $n + 1$ , during each step shown in Fig. (6).

(a) For each one of the qubits 1, 2,  $\dots$ ,  $n + 1$  in step (i), we have, from Eq. (42), that

$$n_g = n_g^{\text{dc}} + n_0^{\text{ac}} \cos(\omega t + \varphi) + n_0^{\text{qu}}(a + a^\dagger), \quad (55)$$

where

$$n_0^{\text{ac}} = C_g V_0 / (2e) = \hbar \Omega / (4E_c),$$

$$n_0^{\text{qu}} = C_g V_0^{\text{qu}} / (2e) = \hbar g / (4E_c).$$

Therefore, the maximal deviation from the degeneracy point for each one of the qubits 1, 2,  $\dots$ ,  $n + 1$  in step (i) is

$$\varepsilon_0 = |n_g^{\text{dc}} + n_0^{\text{ac}} + n_0^{\text{qu}} - 1/2| = \hbar(\Omega + g) / (4E_c). \quad (56)$$

(b) Similarly, one can find that the maximal deviation from the degeneracy point for qubits 2, 3,  $\dots$ ,  $n + 1$  in step (ii) is

$$\varepsilon_1 = \hbar(\Omega' + g') / (4E_c). \quad (57)$$

Note that the deviation from the degeneracy point for qubit 1 is smaller than  $\varepsilon_1$  since  $V_g^{\text{ac}} = 0$  and thus  $n_0^{\text{ac}} = 0$  for qubit 1.

(d) For step (iii), we have  $n_0^{\text{ac}} = \hbar \Omega_1 / (4E_c)$  for qubit 1,  $n_0^{\text{ac}} = \hbar \Omega_r / (4E_c)$  for qubits 2, 3,  $\dots$ ,  $n + 1$ , and  $n_0^{\text{qu}} = 0$ . Thus, it is easy to see that the maximal deviation from the degeneracy point for qubit 1 is

$$\varepsilon_2 = \hbar \Omega_1 / (4E_c), \quad (58)$$

and the deviation from the degeneracy point for qubits 2, 3,  $\dots$ ,  $n + 1$  is

$$\varepsilon_3 = \hbar \Omega_r / (4E_c). \quad (59)$$

In this subsection, we have discussed how to realize the NTCP gate with superconducting charge qubits coupled to a resonator. Note that the proposal here can implement multiqubit gates, while previous proposals (e.g., [49–51]) using superconducting qubits are limited to two-qubit gates.

### C. Possible experimental implementation

In this subsection we discuss some issues which are relevant for future experimental implementation of our proposal. For the method to work, the following conditions must be satisfied: (a) The conditions for the Rabi frequencies  $\Omega$ ,  $\Omega'$ ,  $\Omega_1$ , and  $\Omega_r$ , which were discussed earlier, need to be met. (b) The total operation time

$$t_{\text{op}} = 2\tau + \tau' = 4\pi/|\delta| + 2\pi/\delta' \quad (60)$$

should be much shorter than the energy relaxation time  $T_1$  and the dephasing time  $T_2$  of the qubit and the lifetime of the resonator mode  $\kappa^{-1} = Q/\omega_c$ , where  $Q$  is the (loaded) quality factor of the resonator. (c) The deviations  $\varepsilon_0$ ,  $\varepsilon_1$ ,  $\varepsilon_2$ , and  $\varepsilon_3$  from the degeneracy point need to be small numbers to have the qubits working near the degeneracy point, such that the qubits are less affected by the low-frequency charge noises [52,53]. (d) The direct coupling between SQUIDs needs to be negligible, since this interaction is not intended. It is noted that the direct interaction between SQUIDs can be made negligibly small as long as  $D \gg d$  (where  $D$  is the distance between the two nearest SQUIDs and  $d$  is the linear dimension of each SQUID).

For the sake of definitiveness, let us consider the experimental feasibility of implementing a two-target-qubit CP gate using superconducting charge qubits with parameters listed in Table I [8,54–56]. Note that, in a recent experiment, coupling three superconducting qubits with a transmission line resonator has been demonstrated [57]. For a superconducting one-dimensional standing-wave coplanar waveguide (CPW) transmission line resonator and each qubit placed at an antinode of the resonator mode (Fig. 7), the amplitude of the quantum part of the gate voltage is given by [48]

$$V_0^{\text{qu}} = (\hbar \omega_c)^{1/2} (L C_0)^{-1/2}, \quad (61)$$

TABLE I. Possible experimental parameters of a charge qubit [8,54–56]. Here,  $\Omega_p$  is the typical Rabi frequency available in experiments, and  $\Delta\nu_0$  is the experimental tuning range of the qubit frequency.

Charge qubit	
Gate capacitance	$C_g \sim 1$ aF [54]
Josephson capacitance	$C_{J0} \sim 300$ aF [54]
Charging energy	$E_c/h \sim 32$ GHz [54]
Josephson coupling energy	$E_{J0}/h \sim 5$ GHz [54]
Energy relaxation time	$T_1 \sim 7.3$ $\mu$ s [55]
Dephasing time	$T_2 \sim 500$ ns [55]
Rabi frequency	$\Omega_p/2\pi \sim 300$ MHz [56]
Tuning range of the qubit frequency	$\Delta\nu_0 \sim 350$ MHz [8]

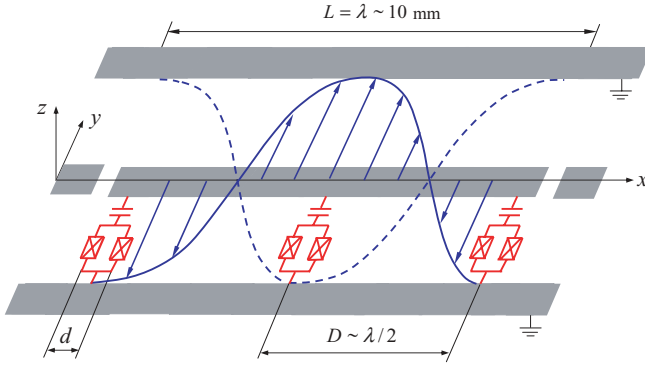


FIG. 7. (Color online) Proposed setup for three qubits and a (gray) standing-wave quasi-one-dimensional coplanar waveguide cavity (not drawn to scale). Each qubit is placed at an antinode of the electric field. The two blue curves represent the standing-wave electric field, along the  $y$  direction.  $D$  is the distance between any two nearest SQUID loops, and  $d$  is the linear dimension of each SQUID loop.

where  $L$  is the length of the resonator and  $c_0$  is the capacitance per unit length of the resonator. Therefore, the coupling constant  $g$  is given by

$$g = 2E_c C_g (\hbar e)^{-1} (\hbar \omega_c)^{1/2} (L c_0)^{-1/2}, \quad (62)$$

showing that  $g$  does not depend on the detuning  $\delta$ . Therefore, we have  $g = g'$ , for which the condition  $-\Omega/\delta = \Omega'/\delta'$  and  $-g/\delta = g'/\delta'$  simply turns to the  $\Omega = \Omega'$  and  $-\delta = \delta'$ . For superconducting charge qubits with parameters given in Table I, and a resonator with the parameters listed in Table II [36,57–59], a simple calculation gives  $g/2\pi \sim 22$  MHz, which is available in experiments (see, e.g., [58]). With a choice of  $-\delta = \delta' = 2g$  [corresponding to  $k = 0$  in Eq. (36)], the total operation time  $t_{\text{op}}$  would be  $\sim 68$  ns, which is much shorter than the dephasing time  $T_2$  and  $\kappa^{-1} \sim 794$  ns for a resonator with  $Q = 10^5$ . Note that a superconducting CPW resonator with a quality factor of  $Q > 10^6$  has been experimentally demonstrated [59].

Based on  $\Omega = \Omega'$ ,  $\Omega_1 = 4\lambda n + \Omega$ , and  $\Omega_r = 4\lambda$  ( $n = 2$  for a two-target-qubit gate), we have  $\Omega'/(2\pi) \sim 330$  MHz,  $\Omega_1/(2\pi) \sim 352$  MHz, and  $\Omega_r/(2\pi) \sim 11$  MHz for a choice of  $\Omega \sim 15g$  [i.e.,  $\Omega/(2\pi) \sim 330$  MHz]. For the Rabi frequencies given here, we obtain  $\varepsilon_0 = \varepsilon_1 \sim 2.75 \times 10^{-3}$ ,  $\varepsilon_2 \sim 2.75 \times 10^{-3}$ , and  $\varepsilon_3 \sim 8.59 \times 10^{-5}$  for a qubit-cavity system with

TABLE II. Possible experimental parameters of a resonator [36,57–59]. Here,  $\Delta\nu_c$  is the experimental tuning range of the resonator frequency.

Resonator	
Resonator frequency	$\omega_c/2\pi = 10$ GHz
Wave length	$\lambda \sim 10$ mm
Length of the resonator	$L = \lambda$
Capacitance per unit length of resonator	$c_0 \sim 0.22$ aF
Effective relative dielectric constant	$\varepsilon_e \sim 9$
Quality factor	$Q \sim 10^5$
Tuning range of the resonator frequency	$\Delta\nu_c \sim 740$ MHz

these parameters. Therefore, the conditions for the qubits to work near the degeneracy point are well satisfied.

For a resonator with  $\omega_c/(2\pi) = 10$  GHz, the wavelength of the resonator mode is  $\lambda \sim 10$  mm. For the charge qubits in a resonator as shown in Fig. 7, the distance between any two nearest SQUIDs is  $D \sim \lambda/2 \sim 5$  mm. Hence, the ratio  $D/d$  would be  $\sim 250$  for  $d = 20$   $\mu\text{m}$ . Note that the dipole field generated by the current in each SQUID ring at a distance  $r \gg d$  decreases as  $r^{-3}$ . Thus, the condition of negligible direct coupling between SQUIDs is well satisfied.

Note that because of  $\omega_0 = 4E_{J0} \cos(\pi\Phi/\Phi_0)/\hbar$ , it can be found that, for charge qubits with the parameters given in Table I, the transition frequency  $\nu_0 = \omega_0/2\pi$  of each qubit varies from  $\nu_0 = 0$  for  $\Phi/\Phi_0 = 1/2$  to  $\nu_0 = 20$  GHz for  $\Phi = 0$ . Therefore, the choice of the resonator frequency here is reasonable. For the choice of  $-\delta = \delta' = 2g$ , the qubit transition frequency  $\nu_0$  would be  $\sim 9.956$  GHz for the detuning  $\delta = -2g$  while it would be  $\sim 10.044$  GHz for the detuning  $\delta' = 2g$ .

Finally, let us estimate the deviation from the degeneracy point induced by tuning the qubit frequency. According to Ref. [30], it is easy to find that when the qubit frequency is tuned from the value  $\nu_0$  at the degeneracy point to the value  $\nu_0 + \Delta\nu_0$  at a nondegeneracy point, the deviation from the degeneracy point for a charge qubit, caused by tuning the qubit frequency, is given by

$$\varepsilon = |n_g - 1/2| = \frac{\sqrt{(\Delta\nu_0)^2 + 8\Delta\nu_0(E_{J0}/h) \cos(\pi\Phi/\Phi_0)}}{8E_c/h}, \quad (63)$$

where  $\varepsilon = 0$  corresponds to  $n_g = 1/2$  (i.e., the case for which the qubit works at the degeneracy point). From Eq. (63), it can be found that when  $\Phi = 0$ , we have  $\varepsilon_{\text{max}} \sim 1.46 \times 10^{-2}$  for  $\Delta\nu_0 \sim 350$  MHz and the charging and the Josephson energies listed in Table I. This result shows that the qubit works near the degeneracy point when tuning the qubit frequency within a range of  $\sim 350$  MHz.

This analysis shows that the realization of a two-target-qubit controlled phase gate is possible using superconducting charge qubits and a resonator. We remark that a quantum-controlled phase gate with a larger number of target qubits can in principle be obtained by increasing the length of the resonator since the total operation time  $t_{\text{op}}$  is independent of the number of target qubits,  $n$ .

## VI. NTCP GATE WITH ATOMS USING ONE CAVITY

Consider  $n + 1$  identical two-level atoms ( $1, 2, \dots, n + 1$ ). The two levels of each atom are labeled by  $|0\rangle$  and  $|1\rangle$ . The transition frequency of each atom is denoted as  $\omega_0$ . Each atom is trapped in the periodic potential of a one-dimensional optical lattice and can be loaded into or moved out of the cavity by translating the optical lattice [20,45,46]. The NTCP gate can be realized using a procedure illustrated in Fig. 8. The operations shown in Fig. 8 are as follows:

Figure 8(a): Move atoms  $1, 2, \dots, n + 1$  into the cavity and then apply a classical pulse (with an initial phase  $\varphi = \pi$  and frequency  $\omega = \omega_0$ ) to the atoms. The cavity mode is coupled to the  $|0\rangle \rightarrow |1\rangle$  transition of each atom, with a detuning

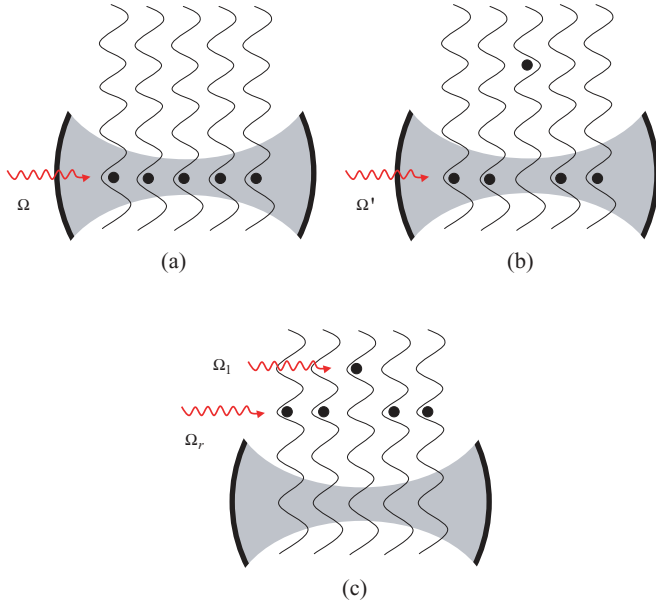


FIG. 8. (Color online) Proposed setup for an NTCP gate with  $n + 1$  identical neutral atoms and a cavity. For simplicity, only five atoms are drawn here. Each atom can be either loaded into the cavity or moved out of the cavity by one-dimensional translating optical lattices [20,45,46]. The atom in the middle represents atom 1 (the control qubit), while the remaining atoms play the role of target qubits.

$\delta = \omega_0 - \omega_c < 0$ , which can be achieved by prior adjustment of the cavity mode frequency [35]. The time-evolution operator for this operation is the  $U$  in Eq. (19) for an interaction time  $\tau = -2\pi/\delta$ .

Figure 8(b): Move atoms  $1, 2, \dots, n + 1$  out of the cavity and then adjust the cavity mode frequency. After adjusting the cavity mode frequency, move atoms  $2, 3, \dots, n + 1$  back into the cavity and then apply a classical pulse (with  $\varphi = 0$  and  $\omega = \omega_0$ ) to them. The cavity mode frequency is adjusted such that the cavity mode is coupled to the  $|0\rangle \rightarrow |1\rangle$  transition of atoms  $2, 3, \dots, n + 1$ , with a detuning  $\delta' = \omega_0 - \omega_c > 0$ . The time-evolution operator for this operation is the  $U'$  in Eq. (26) for an interaction time  $\tau' = 2\pi/\delta'$ .

Figure 8(c): Move atoms  $2, 3, \dots, n + 1$  out of the cavity. Apply a classical pulse (with  $\varphi = 0$  and  $\omega = \omega_0$ ) to the control atom 1 and a classical pulse (with the same initial phase and frequency) to the target atoms  $(2, 3, \dots, n + 1)$ . The Rabi frequency for the pulse applied to atom 1 is  $\Omega_1$ , while the Rabi frequency for the pulses applied to atoms  $2, 3, \dots, n + 1$  is  $\Omega_r$ . This operation is described by the operator  $\tilde{U}$  in Eq. (28) for an interaction time  $\tau$ .

The three time-evolution operators  $U$ ,  $U'$ , and  $\tilde{U}$  here are the same as those obtained from each step in Sec. IV A. Therefore, as long as the conditions given in Sec. IV A are met, an NTCP gate described by Eq. (39) is implemented with the  $n + 1$  atoms. Namely, after the operations shown in Fig. 8,  $n$  two-qubit controlled phase gates, each described by the unitary transformation in Eq. (1), are performed on the atom pairs  $(1, 2)$ ,  $(1, 3)$ ,  $\dots$ , and  $(1, n + 1)$ , respectively. Note that each pair contains the same control qubit (atom 1) but a different target qubit (atom  $2, 3, \dots$ , or  $n + 1$ ).

As shown, the present scheme for implementing the NTCP gate with atoms has the following features: (a) No adjustment of the level spacings for each atom is required during the entire operation; (b) only one cavity is required; (c) the cavity mode can be initially in an arbitrary state; and (d) the operation time does not depend on the number of atoms.

For our scheme to work, the total operation time  $t_{\text{op}} = \tau + \tau' + \tau_a + 4\tau_m$  should be much smaller than the cavity decay time  $\kappa^{-1}$ , so that the cavity dissipation is negligible. Here,  $\tau_a$  is the typical time required for adjusting the cavity mode frequency during step (ii), and  $\tau_m$  is the typical time required for moving atoms into or out of the cavity. In addition, the  $t_{\text{op}}$  needs to be much smaller than the energy relaxation time of level  $|1\rangle$ , such that the decoherence induced by the spontaneous decay of the level  $|1\rangle$  is negligible. In principle, these conditions can be satisfied by choosing a cavity with a high quality factor  $Q$  and atoms with a sufficiently long energy relaxation time.

To investigate the experimental feasibility of this proposal, let us consider Rydberg atoms with principal quantum numbers 50 and 51 (respectively, corresponding to the levels  $|0\rangle$  and  $|1\rangle$ ). The  $|0\rangle \leftrightarrow |1\rangle$  transition frequency is  $\omega_0/2\pi \sim 51.1$  GHz, the energy relaxation time of the level  $|1\rangle$  is  $T_r \sim 3 \times 10^{-2}$  s, and the coupling constant is  $g = 2\pi \times 50$  KHz [35,60]. Now set  $-\delta = \delta' = 2g$ , and assume  $g \sim g'$ . With the choice of these parameters, the time needed for the entire operation is  $t_{\text{op}} \sim 65 \mu\text{s}$  for  $\tau_a = \tau_m \sim 1 \mu\text{s}$ , which is much shorter than  $T_r$ . The cavity mode frequency is  $\omega_c/2\pi \sim 51.2$  GHz for the negative qubit detuning  $\delta = -2g$  while it is  $\sim 51$  GHz for the positive qubit detuning  $\delta' = 2g$ . To estimate the lifetime of the cavity photon, we here consider the conservative case of a larger cavity frequency  $\omega_c/2\pi \sim 51.2$  GHz, for which the lifetime of the cavity photon is  $T_c = Q/\omega_c \sim 622 \mu\text{s}$  for a cavity with  $Q = 2 \times 10^8$ , which is much larger than the total operation time  $t_{\text{op}}$ . Note that cavities with a high  $Q$  ( $\sim 10^{10}$ ) have been demonstrated in experiments [61]. Thus, the present proposal might be realizable using current cavity QED setups.

## VII. CONCLUSIONS

We have presented two different methods for the proposed NTCP gate implementation. The two methods are quite general and can be applied to physical systems such as trapped atoms, quantum dots, and superconducting qubits. For the two methods, we have provided guidelines on how to protect multilevel qubits from leaking out of the computational subspace.

Using a concrete example, we have shown how to apply the first method to implement the NTCP gate with superconducting qubits coupled to a resonator. In addition, we have discussed the experimental feasibility of performing a two-target-qubit controlled phase gate with superconducting qubits coupled to a one-dimensional transmission line resonator. Our analysis shows that the realization of this gate is possible within current technologies. How well this gate would work in light of experimental errors should be further investigated elsewhere for each particular setup or implementation. This is beyond the scope of this theoretical work.

We have shown how to extend the second method to implement the NTCP gate with trapped atomic qubits by using one cavity. Interestingly, as shown here, there is no need to adjust the level spacings of atoms during the entire operation, and decoupling of atoms with the cavity can be easily achieved by just moving atoms out of the cavity.

In summary, we have presented a general proposal to implement an NTCP gate with qubits in a cavity or coupled to a resonator. The present proposal has the following features: (i) The  $n$  two-qubit CP gates involved in the NTCP gate can be simultaneously performed; (ii) the operation time required for the gate implementation is independent of the number of the qubits and thus it does not increase with the number of qubits; (iii) the gate is insensitive to the initial state of the cavity mode, and therefore no preparation for a specified initial state of the cavity mode is needed; (iv) no measurement on the qubits or the cavity mode is needed and thus the operation is simplified, and (v) the gate realization requires only three operational steps.

#### ACKNOWLEDGMENTS

FN and CPY acknowledge partial support from the National Security Agency (NSA), Laboratory for Physical Sciences (LPS), US Army Research Office (USARO), National Science Foundation (NSF) under Grant No. 0726909, JSPS-RFBR Contract No. 09-02-92114, MEXT Kakenhi on Quantum Cybernetics, and FIRST (Funding Program for Innovative R&D on S&T). YXL is supported by the National Natural Science Foundation of China under Grant Nos. 10975080 and 60836001. We are very grateful to an anonymous referee for numerous suggestions, which significantly improved the presentation of our results.

#### APPENDIX: HOW TO PROTECT QUBITS FROM LEAKING TO HIGHER ENERGY LEVELS

Let us now discuss how to protect qubits from leaking out of the computational subspace in the presence of more qubit levels. Generally speaking, we need to consider two situations, which are here denoted as cases  $L$  and  $S$ . For case  $L$ , the level spacing between the level  $|1\rangle$  and the level  $|2\rangle$  (the first level above  $|1\rangle$ ) is *larger* than the level spacing between the levels  $|0\rangle$  and  $|1\rangle$ . Namely, for case  $L$ ,  $(E_2 - E_1) > (E_1 - E_0)$ , where  $E_0$ ,  $E_1$ , and  $E_2$  are the energy eigenvalues of the levels  $|0\rangle$ ,  $|1\rangle$ , and  $|2\rangle$ . For case  $S$ , the level spacing between the levels  $|1\rangle$  and  $|2\rangle$  is *smaller* than that between the levels  $|0\rangle$  and  $|1\rangle$ . Namely,  $(E_2 - E_1) < (E_1 - E_0)$ . For solid-state qubits, case  $L$  exists for superconducting charge qubits and flux qubits [31]; case  $S$  can be applied to superconducting phase qubits [33]. For atomic qubits, the level structures for both cases  $L$  and  $S$  are available.

Here and in the following, we define  $\Delta_2 = (E_2 - E_1)/\hbar - \omega_c$ ,  $\Delta_3 = (E_3 - E_1)/\hbar - \omega_c$ , and  $\Delta_a = (E_a - E_1)/\hbar - \omega_c$ , as the large detuning of the cavity mode with the  $|1\rangle \leftrightarrow |2\rangle$  transition, the large detuning of the cavity mode with the  $|1\rangle \leftrightarrow |3\rangle$  transition, and the large detuning of the cavity mode with the  $|1\rangle \leftrightarrow |a\rangle$  transition, respectively, where  $E_a$  is the energy eigenvalue of level  $|a\rangle$ .

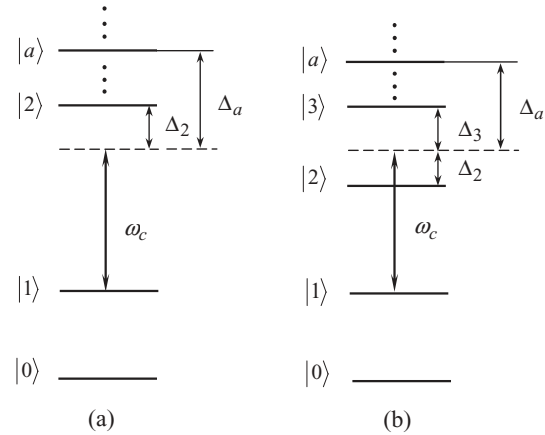


FIG. 9. Large detuning of the cavity mode with the transition between energy levels. Figure (a) corresponds to the case  $L$ , while figure (b) corresponds to case  $S$ . The dots above level  $|2\rangle$  in (a) and level  $|3\rangle$  in (b) represent other energy levels.

#### A. Case $L$ : $(E_2 - E_1) > (E_1 - E_0)$

For case  $L$ , let us consider Fig. 9(a), where the dashed line falls within the range between the levels  $|1\rangle$  and  $|2\rangle$  when the cavity mode is slightly detuned from the  $|0\rangle \leftrightarrow |1\rangle$  transition. Therefore, a large detuning  $\Delta_2$  is needed to avoid the transition from the level  $|1\rangle$  to the level  $|2\rangle$ . Note also that as long as this large detuning is met, no transition from level  $|1\rangle$  to the higher energy level above the level  $|2\rangle$  happens. To explain this, let us consider an arbitrary level  $|a\rangle$  above level  $|2\rangle$  [Fig. 9(a)]. Since the detuning  $\Delta_a$  is larger than the detuning  $\Delta_2$ , then the large detuning regime for  $\Delta_a$  is automatically satisfied when  $\Delta_2$  is large. As a result, the transition from the level  $|1\rangle$  to the level  $|a\rangle$  will not be induced by the cavity mode. In addition, the excitation of the level  $|a\rangle$ , induced by its coupling to the level  $|2\rangle$  via the cavity mode, does not occur when the level  $|2\rangle$  is unpopulated. Hence, as long as the large detuning  $\Delta_2$  is satisfied, no level above  $|1\rangle$  will be populated and therefore the leak out of the computational subspace is suppressed.

#### B. Case $S$ : $(E_2 - E_1) < (E_1 - E_0)$

For case  $S$ , let us consider Fig. 9(b), where the dashed line falls within the range between the levels  $|2\rangle$  and  $|3\rangle$ , when the cavity mode is slightly detuned from the  $|0\rangle \leftrightarrow |1\rangle$  transition. This can be achieved, for example, for superconducting qubits by appropriately choosing the device parameters and/or adjusting the external parameters to control the level structures. From Fig. 9(b), it can be seen that a large detuning  $\Delta_2$  and a large detuning  $\Delta_3$  are needed to avoid the transition from the level  $|1\rangle$  to the level  $|2\rangle$  or the level  $|3\rangle$ . Note also that as long as these two large detunings are met, no transition from the level  $|1\rangle$  to the higher energy level above the level  $|3\rangle$  occurs. To understand this, let us consider an arbitrary level  $|a\rangle$  above level  $|3\rangle$  [Fig. 9(b)]. Note that the detuning  $\Delta_a$  is larger than the detuning  $\Delta_3$ . Therefore, the large detuning regime for  $\Delta_a$  is automatically satisfied when the cavity mode is largely detuned from the  $|1\rangle \leftrightarrow |3\rangle$  transition. As a result, the transition from level  $|1\rangle$  to level  $|a\rangle$  will not be induced by the cavity mode. In addition, the excitation of the level  $|a\rangle$ , caused by its coupling

to the level  $|2\rangle$  or  $|3\rangle$  via the cavity mode, will not happen when levels  $|2\rangle$  and  $|3\rangle$  are unpopulated. Hence, as long as the large detunings  $\Delta_2$  and  $\Delta_3$  are met, the levels above  $|1\rangle$  will not be excited by the cavity mode.

We now give a quantitative analysis on the effect of the finite detuning of the qubit frequencies with the cavity mode. For simplicity, we consider the case where the cavity mode is in a single-photon state and the qubit is in the state  $|1\rangle$ . It is estimated that the occupation probability  $p_2$  for level  $|2\rangle$  and the occupation probability  $p_3$  for level  $|3\rangle$  (induced by the photon) would be on the order of  $4g_{12}^2/(4g_{12}^2 + \Delta_2^2)$  and  $4g_{13}^2/(4g_{13}^2 + \Delta_3^2)$ , respectively. Here,  $g_{12}$  is the coupling constant between the cavity mode and the  $|1\rangle \leftrightarrow |2\rangle$  transition,

while  $g_{13}$  is the coupling constant between the cavity mode and the  $|1\rangle \leftrightarrow |3\rangle$  transition. With a choice of  $\Delta_2 = 10g_{12}$  and  $\Delta_3 = 10g_{13}$ , we have  $p_2, p_3 \sim 0.04$ , which can be further reduced by increasing the detuning  $\Delta_2$  or  $\Delta_3$ . Therefore, the population probability of the level  $|2\rangle$  or  $|3\rangle$  of the qubit can be made negligible by choosing the detuning appropriately.

When the coupling constants  $g_{12}$  and  $g_{13}$  are on the order of  $g$  (where  $g$  is the coupling constant between the  $|0\rangle \leftrightarrow |1\rangle$  transition and the cavity mode), we have  $\Delta_2, \Delta_3 \sim 10g$ . For  $g/2\pi \sim 22$  MHz (given in Sec. V C), we obtain  $\Delta_2/2\pi, \Delta_3/2\pi \sim 220$  MHz, which is within the experimentally tuning range  $\sim 350$  MHz of the qubit frequency listed in Table I.

- 
- [1] C. Monroe, D. M. Meekhof, B. E. King, W. M. Itano, and D. J. Wineland, *Phys. Rev. Lett.* **75**, 4714 (1995).
- [2] J. A. Jones, M. Mosca, and R. H. Hansen, *Nature (London)* **393**, 344 (1998).
- [3] X. Li, Y. Wu, D. Steel, D. Gammon, T. H. Stievater, D. D. Katzer, D. Park, C. Piermarocchi, and L. J. Sham, *Science* **301**, 809 (2003).
- [4] T. Yamamoto, Yu. A. Pashkin, O. Astafiev, Y. Nakamura, and J. S. Tsai, *Nature (London)* **425**, 941 (2003).
- [5] J. H. Plantenberg, P. C. de Groot, C. J. P. M. Harmans, and J. E. Mooij, *Nature (London)* **447**, 836 (2007).
- [6] R. C. Bialczak *et al.*, e-print arXiv:0910.1118.
- [7] J. Majer *et al.*, *Nature (London)* **449**, 443 (2007).
- [8] P. J. Leek, S. Filipp, P. Maurer, M. Baur, R. Bianchetti, J. M. Fink, M. Göppl, L. Steffen, and A. Wallraff, *Phys. Rev. B* **79**, 180511(R) (2009).
- [9] D. I. Schuster, A. Wallraff, A. Blais, L. Frunzio, R.-S. Huang, J. Majer, S. M. Girvin, and R. J. Schoelkopf, *Phys. Rev. Lett.* **94**, 123602 (2005).
- [10] J. Q. You and F. Nori, *Phys. Rev. B* **68**, 064509 (2003).
- [11] J. Q. You, J. S. Tsai, and F. Nori, *Phys. Rev. B* **68**, 024510 (2003).
- [12] C. P. Yang, S. I. Chu, and S. Han, *Phys. Rev. A* **67**, 042311 (2003).
- [13] P. Zhang, Z. D. Wang, J. D. Sun, and C. P. Sun, *Phys. Rev. A* **71**, 042301 (2005).
- [14] S. L. Zhu, Z. D. Wang, and P. Zanardi, *Phys. Rev. Lett.* **94**, 100502 (2005).
- [15] Z. B. Feng, *Phys. Rev. A* **78**, 032325 (2008).
- [16] T. Monz, K. Kim, W. Hänsel, M. Riebe, A. S. Villar, P. Schindler, M. Chwalla, M. Hennrich, and R. Blatt, *Phys. Rev. Lett.* **102**, 040501 (2009).
- [17] A. Barenco, C. H. Bennett, R. Cleve, D. P. DiVincenzo, N. Margolus, P. Shor, T. Sleator, J. A. Smolin, and H. Weinfurter, *Phys. Rev. A* **52**, 3457 (1995).
- [18] M. Möttönen, J. J. Vartiainen, V. Bergholm, and M. M. Salomaa, *Phys. Rev. Lett.* **93**, 130502 (2004).
- [19] X. Wang, A. Sørensen, and K. Mølmer, *Phys. Rev. Lett.* **86**, 3907 (2001).
- [20] L. M. Duan, B. Wang, and H. J. Kimble, *Phys. Rev. A* **72**, 032333 (2005).
- [21] X. M. Lin, Z. W. Zhou, M. Y. Ye, Y. F. Xiao, and G. C. Guo, *Phys. Rev. A* **73**, 012323 (2006).
- [22] C. P. Yang and S. Han, *Phys. Rev. A* **72**, 032311 (2005).
- [23] P. W. Shor, in *Proceedings of the 35th Annual Symposium on Foundations of Computer Science*, edited by S. Goldwasser (IEEE Computer Society Press, Los Alamitos, CA, 1994), pp. 124–134.
- [24] L. K. Grover, *Phys. Rev. Lett.* **80**, 4329 (1998).
- [25] P. W. Shor, *Phys. Rev. A* **52**, R2493 (1995); A. M. Steane, *Phys. Rev. Lett.* **77**, 793 (1996).
- [26] M. Šašura and V. Buzek, *Phys. Rev. A* **64**, 012305 (2001).
- [27] F. Gaitan, *Quantum Error Correction and Fault Tolerant Quantum Computing* (CRC Press, USA, 2008).
- [28] T. Beth and M. Rötteler, *Quantum Information* (Springer, Berlin, 2001), Vol. 173, Ch. 4, p. 96.
- [29] S. L. Braunstein, V. Buzek, and M. Hillery, *Phys. Rev. A* **63**, 052313 (2001).
- [30] Y. Makhlin, G. Schön, and A. Shnirman, *Rev. Mod. Phys.* **73**, 357 (2001).
- [31] J. Q. You and F. Nori, *Phys. Today* **58**, 42 (2005).
- [32] J. Clarke and F. K. Wilhelm, *Nature (London)* **453**, 1031 (2008).
- [33] M. Neeley, M. Ansmann, R. C. Bialczak, M. Hofheinz, N. Katz, E. Lucero, A. O’Connell, H. Wang, A. N. Cleland, and J. M. Martinis, *Nature Phys.* **4**, 523 (2008); A. M. Zagoskin, S. Ashhab, J. R. Johansson, and F. Nori, *Phys. Rev. Lett.* **97**, 077001 (2006).
- [34] For quantum dots, the level spacings can be changed via adjusting the external electronic field. For details, see P. Pradhan, M. P. Anantram, and K. L. Wang, e-print arXiv:quant-ph/0002006.
- [35] M. Brune, E. Hagley, J. Dreyer, X. Maitre, A. Maali, C. Wunderlich, J. M. Raimond, and S. Haroche, *Phys. Rev. Lett.* **77**, 4887 (1996).
- [36] M. Sandberg, C. M. Wilson, F. Persson, T. Bauch, G. Johansson, V. Shumeiko, T. Duty, and P. Delsing, *Appl. Phys. Lett.* **92**, 203501 (2008).
- [37] A. Palacios-Laloy, F. Nguyen, F. Mallet, P. Bertet, D. Vion, and D. Esteve, *J. Low Temp. Phys.* **151**, 1034 (2008).
- [38] J. R. Johansson, G. Johansson, C. M. Wilson, and F. Nori, *Phys. Rev. Lett.* **103**, 147003 (2009).
- [39] J. Q. Liao, Z. R. Gong, L. Zhou, Y. X. Liu, C. P. Sun, and F. Nori, *Phys. Rev. A* **81**, 042304 (2010).
- [40] S. B. Zheng, *Phys. Rev. A* **66**, 060303(R) (2002).
- [41] E. Solano, G. S. Agarwal, and H. Walther, *Phys. Rev. Lett.* **90**, 027903 (2003).
- [42] Z. J. Deng, M. Feng, and K. L. Gao, *Phys. Rev. A* **72**, 034306 (2005).

- [43] A. Sørensen and K. Mølmer, *Phys. Rev. A* **62**, 022311 (2000).
- [44] Y. D. Wang, P. Zhang, D. L. Zhou, and C. P. Sun, *Phys. Rev. B* **70**, 224515 (2004).
- [45] A. Beige, D. Braun, B. Tregenna, and P. L. Knight, *Phys. Rev. Lett.* **85**, 1762 (2000).
- [46] J. A. Sauer, K. M. Fortier, M. S. Chang, C. D. Hamley, and M. S. Chapman, *Phys. Rev. A* **69**, 051804(R) (2004).
- [47] M. Hofheinz *et al.*, *Nature (London)* **459**, 546 (2009).
- [48] A. Blais, R. S. Huang, A. Wallraff, S. M. Girvin, and R. J. Schoelkopf, *Phys. Rev. A* **69**, 062320 (2004).
- [49] J. Q. You, J. S. Tsai, and F. Nori, *Phys. Rev. Lett.* **89**, 197902 (2002).
- [50] J. Q. You, Y. Nakamura, and F. Nori, *Phys. Rev. B* **71**, 024532 (2005).
- [51] Y. X. Liu, L. F. Wei, J. R. Johansson, J. S. Tsai, and F. Nori, *Phys. Rev. B* **76**, 144518 (2007).
- [52] Y. Nakamura, Y. A. Pashkin, T. Yamamoto, and J. S. Tsai, *Phys. Rev. Lett.* **88**, 047901 (2002).
- [53] D. Vion, A. Aassime, A. Cottet, P. Joyez, H. Pothier, C. Urbina, D. Esteve, and M. H. Devoret, *Science* **296**, 886 (2002).
- [54] O. Astafiev, Y. A. Pashkin, Y. Nakamura, T. Yamamoto, and J. S. Tsai, *Phys. Rev. Lett.* **93**, 267007 (2004).
- [55] A. Wallraff, D. I. Schuster, A. Blais, L. Frunzio, J. Majer, M. H. Devoret, S. M. Girvin, and R. J. Schoelkopf, *Phys. Rev. Lett.* **95**, 060501 (2005).
- [56] M. Baur, S. Filipp, R. Bianchetti, J. M. Fink, M. Göppl, L. Steffen, P. J. Leek, A. Blais, and A. Wallraff, *Phys. Rev. Lett.* **102**, 243602 (2009).
- [57] J. M. Fink, R. Bianchetti, M. Baur, M. Göppl, L. Steffen, S. Filipp, P. J. Leek, A. Blais, and A. Wallraff, *Phys. Rev. Lett.* **103**, 083601 (2009).
- [58] D. I. Schuster *et al.*, *Nature (London)* **445**, 515 (2007).
- [59] P. K. Day, H. G. LeDuc, B. A. Mazin, A. Vayonakis, and J. Zmuidzinas, *Nature (London)* **425**, 817 (2003).
- [60] S. Osnaghi, P. Bertet, A. Auffeves, P. Maioli, M. Brune, J. M. Raimond, and S. Haroche, *Phys. Rev. Lett.* **87**, 037902 (2001).
- [61] S. Kuhr *et al.*, *Appl. Phys. Lett.* **90**, 164101 (2007).